

# Neutrino Oscillation Physics Potential of the T2K Experiment

K. Abe<sup>47</sup>, J. Adam<sup>33</sup>, H. Aihara<sup>46,23</sup>, T. Akiri<sup>9</sup>, C. Andreopoulos<sup>45</sup>, S. Aoki<sup>24</sup>, A. Ariga<sup>2</sup>, S. Assylbekov<sup>8</sup>, D. Autiero<sup>29</sup>, M. Barbi<sup>40</sup>, G.J. Barker<sup>55</sup>, G. Barr<sup>36</sup>, P. Bartet-Friburg<sup>37</sup>, M. Bass<sup>8</sup>, M. Batkiewicz<sup>13</sup>, F. Bay<sup>11</sup>, V. Berardi<sup>18</sup>, B.E. Berger<sup>8,23</sup>, S. Berkman<sup>4</sup>, S. Bhadra<sup>59</sup>, F.d.M. Blaszczyk<sup>28</sup>, A. Blondel<sup>12</sup>, C. Bojecho<sup>52</sup>, S. Bordini<sup>15</sup>, S.B. Boyd<sup>55</sup>, D. Brailsford<sup>17</sup>, A. Bravar<sup>12</sup>, C. Bronner<sup>23</sup>, N. Buchanan<sup>8</sup>, R.G. Calland<sup>27</sup>, J. Caravaca Rodríguez<sup>15</sup>, S.L. Cartwright<sup>43</sup>, R. Castillo<sup>15</sup>, M.G. Catanesi<sup>18</sup>, A. Cervera<sup>16</sup>, D. Cherdack<sup>8</sup>, G. Christodoulou<sup>27</sup>, A. Clifton<sup>8</sup>, J. Coleman<sup>27</sup>, S.J. Coleman<sup>7</sup>, G. Collazuol<sup>20</sup>, K. Connolly<sup>56</sup>, L. Cremonesi<sup>39</sup>, A. Dabrowska<sup>13</sup>, I. Danko<sup>38</sup>, R. Das<sup>8</sup>, S. Davis<sup>56</sup>, P. de Perio<sup>50</sup>, G. De Rosa<sup>19</sup>, T. Dealtry<sup>45,36</sup>, S.R. Dennis<sup>55,45</sup>, C. Densham<sup>45</sup>, D. Dewhurst<sup>36</sup>, F. Di Lodovico<sup>39</sup>, S. Di Luise<sup>11</sup>, O. Drapier<sup>10</sup>, T. Duboyski<sup>39</sup>, K. Duffy<sup>36</sup>, J. Dumarchez<sup>37</sup>, S. Dytman<sup>38</sup>, M. Dziewiecki<sup>54</sup>, S. Emery-Schrenk<sup>6</sup>, A. Ereditato<sup>2</sup>, L. Escudero<sup>16</sup>, T. Feusels<sup>4</sup>, A.J. Finch<sup>26</sup>, G.A. Fiorentini<sup>59</sup>, M. Friend<sup>14,†</sup>, Y. Fujii<sup>14,†</sup>, Y. Fukuda<sup>31</sup>, A.P. Furmanski<sup>55</sup>, V. Galymov<sup>29</sup>, A. Garcia<sup>15</sup>, S. Giffin<sup>40</sup>, C. Giganti<sup>37</sup>, K. Gilje<sup>33</sup>, D. Goeldi<sup>2</sup>, T. Golan<sup>58</sup>, M. Gonin<sup>10</sup>, N. Grant<sup>26</sup>, D. Gudin<sup>22</sup>, D.R. Hadley<sup>55</sup>, L. Haegel<sup>12</sup>, A. Haesler<sup>12</sup>, M.D. Haigh<sup>55</sup>, P. Hamilton<sup>17</sup>, D. Hansen<sup>38</sup>, T. Hara<sup>24</sup>, M. Hartz<sup>23,51</sup>, T. Hasegawa<sup>14,†</sup>, N.C. Hastings<sup>40</sup>, T. Hayashino<sup>25</sup>, Y. Hayato<sup>47,23</sup>, C. Hearty<sup>4,‡</sup>, R.L. Helmer<sup>51</sup>, M. Hierholzer<sup>2</sup>, J. Hignight<sup>33</sup>, A. Hillairet<sup>52</sup>, A. Himmel<sup>9</sup>, T. Hiraki<sup>25</sup>, S. Hirota<sup>25</sup>, J. Holeczek<sup>44</sup>, S. Horikawa<sup>11</sup>, K. Huang<sup>25</sup>, A.K. Ichikawa<sup>25,\*</sup>, K. Ieki<sup>25</sup>, M. Ieva<sup>15</sup>, M. Ikeda<sup>47</sup>, J. Imber<sup>33</sup>, J. Insler<sup>28</sup>, T.J. Irvine<sup>48</sup>, T. Ishida<sup>14,†</sup>, T. Ishii<sup>14,†</sup>, E. Iwai<sup>14</sup>, K. Iwamoto<sup>41</sup>, K. Iyogi<sup>47</sup>, A. Izmaylov<sup>16,22</sup>, A. Jacob<sup>36</sup>, B. Jamieson<sup>57</sup>, R.A. Johnson<sup>7</sup>, S. Johnson<sup>7</sup>, J.H. Jo<sup>33</sup>, P. Jonsson<sup>17</sup>, C.K. Jung<sup>33,§</sup>, M. Kabirnezhad<sup>32</sup>, A.C. Kaboth<sup>17</sup>, T. Kajita<sup>48,§</sup>, H. Kakuno<sup>49</sup>, J. Kameda<sup>47</sup>, Y. Kanazawa<sup>46</sup>, D. Karlen<sup>52,51</sup>, I. Karpikov<sup>22</sup>, T. Katori<sup>39</sup>, E. Kearns<sup>3,23</sup>, M. Khabibullin<sup>22</sup>, A. Khotjantsev<sup>22</sup>, D. Kielczewska<sup>53</sup>, T. Kikawa<sup>25</sup>, A. Kilinski<sup>32</sup>, J. Kim<sup>4</sup>, S. King<sup>39</sup>, J. Kisiel<sup>44</sup>, P. Kitching<sup>1</sup>, T. Kobayashi<sup>14,†</sup>, L. Koch<sup>42</sup>, T. Koga<sup>46</sup>, A. Kolaceke<sup>40</sup>, A. Konaka<sup>51</sup>, L.L. Kormos<sup>26</sup>, A. Korzenev<sup>12</sup>, Y. Koshio<sup>34,§</sup>, W. Kropp<sup>5</sup>, H. Kubo<sup>25</sup>, Y. Kudenko<sup>22,¶</sup>, R. Kurjata<sup>54</sup>, T. Kutter<sup>28</sup>, J. Lagoda<sup>32</sup>, K. Laihem<sup>42</sup>, I. Lamont<sup>26</sup>, E. Larkin<sup>55</sup>, M. Laveder<sup>20</sup>, M. Lawe<sup>43</sup>, M. Lazos<sup>27</sup>, T. Lindner<sup>51</sup>, C. Lister<sup>55</sup>, R.P. Litchfield<sup>55</sup>, A. Longhin<sup>20</sup>, J.P. Lopez<sup>7</sup>, L. Ludovici<sup>21</sup>, L. Magaletti<sup>18</sup>, K. Mahn<sup>30</sup>, M. Malek<sup>17</sup>, S. Manly<sup>41</sup>, A.D. Marino<sup>7</sup>, J. Marteau<sup>29</sup>, J.F. Martin<sup>50</sup>, P. Martins<sup>39</sup>, S. Martynenko<sup>22</sup>, T. Maruyama<sup>14,†</sup>, V. Matveev<sup>22</sup>, K. Mavrokoridis<sup>27</sup>, E. Mazzucato<sup>6</sup>, M. McCarthy<sup>4</sup>, N. McCauley<sup>27</sup>, K.S. McFarland<sup>41</sup>, C. McGrew<sup>33</sup>, A. Mefodiev<sup>22</sup>, C. Metelko<sup>27</sup>, M. Mezzetto<sup>20</sup>, P. Mijakowski<sup>32</sup>, C.A. Miller<sup>51</sup>, A. Minamino<sup>25</sup>, O. Mineev<sup>22</sup>, A. Missert<sup>7</sup>, M. Miura<sup>47,§</sup>, S. Moriyama<sup>47,§</sup>, Th.A. Mueller<sup>10</sup>, A. Murakami<sup>25</sup>, M. Murdoch<sup>27</sup>, S. Murphy<sup>11</sup>, J. Myslik<sup>52</sup>, T. Nakadaira<sup>14,†</sup>, M. Nakahata<sup>47,23</sup>, K.G. Nakamura<sup>25</sup>, K. Nakamura<sup>23,14,†</sup>, S. Nakayama<sup>47,§</sup>, T. Nakaya<sup>25,23</sup>, K. Nakayoshi<sup>14,†</sup>, C. Nantais<sup>4</sup>, C. Nielsen<sup>4</sup>, M. Nirkko<sup>2</sup>, K. Nishikawa<sup>14,†</sup>, Y. Nishimura<sup>48</sup>, J. Nowak<sup>26</sup>, H.M. O'Keefe<sup>26</sup>, R. Ohta<sup>14,†</sup>, K. Okumura<sup>48,23</sup>, T. Okusawa<sup>35</sup>, W. Oryszczak<sup>53</sup>, S.M. Oser<sup>4</sup>, T. Ovsyannikova<sup>22</sup>, R.A. Owen<sup>39</sup>, Y. Oyama<sup>14,†</sup>, V. Palladino<sup>19</sup>, J.L. Palomino<sup>33</sup>, V. Paolone<sup>38</sup>, D. Payne<sup>27</sup>, O. Perevozchikov<sup>28</sup>, J.D. Perkin<sup>43</sup>, Y. Petrov<sup>4</sup>, L. Pickard<sup>43</sup>,

E.S. Pinzon Guerra<sup>59</sup>, C. Pistillo<sup>2</sup>, P. Plonski<sup>54</sup>, E. Poplawska<sup>39</sup>, B. Popov<sup>37,\*\*</sup>,  
M. Posiadala-Zezula<sup>53</sup>, J.-M. Poutissou<sup>51</sup>, R. Poutissou<sup>51</sup>, P. Przewlocki<sup>32</sup>,  
B. Quilain<sup>10</sup>, E. Radicioni<sup>18</sup>, P.N. Ratoff<sup>26</sup>, M. Ravonel<sup>12</sup>, M.A.M. Rayner<sup>12</sup>,  
A. Redij<sup>2</sup>, M. Reeves<sup>26</sup>, E. Reinherz-Aronis<sup>8</sup>, C. Riccio<sup>19</sup>, P.A. Rodrigues<sup>41</sup>, P. Rojas<sup>8</sup>,  
E. Rondio<sup>32</sup>, S. Roth<sup>42</sup>, A. Rubbia<sup>11</sup>, D. Ruterbories<sup>41</sup>, R. Sacco<sup>39</sup>, K. Sakashita<sup>14,†</sup>,  
F. Sánchez<sup>15</sup>, F. Sato<sup>14</sup>, E. Scantamburlo<sup>12</sup>, K. Scholberg<sup>9,§</sup>, S. Schoppmann<sup>42</sup>,  
J. Schwehr<sup>8</sup>, M. Scott<sup>51</sup>, Y. Seiya<sup>35</sup>, T. Sekiguchi<sup>14,†</sup>, H. Sekiya<sup>47,§</sup>, D. Sgalaberna<sup>11</sup>,  
R. Shah<sup>45,36</sup>, F. Shaker<sup>57</sup>, M. Shiozawa<sup>47,23</sup>, S. Short<sup>39</sup>, Y. Shustrov<sup>22</sup>, P. Sinclair<sup>17</sup>,  
B. Smith<sup>17</sup>, M. Smy<sup>5</sup>, J.T. Sobczyk<sup>58</sup>, H. Sobel<sup>5,23</sup>, M. Sorel<sup>16</sup>, L. Southwell<sup>26</sup>,  
P. Stamoulis<sup>16</sup>, J. Steinmann<sup>42</sup>, B. Still<sup>39</sup>, Y. Suda<sup>46</sup>, A. Suzuki<sup>24</sup>, K. Suzuki<sup>25</sup>,  
S.Y. Suzuki<sup>14,†</sup>, Y. Suzuki<sup>23</sup>, R. Tacik<sup>40,51</sup>, M. Tada<sup>14,†</sup>, S. Takahashi<sup>25</sup>, A. Takeda<sup>47</sup>,  
Y. Takeuchi<sup>24,23</sup>, H.K. Tanaka<sup>47,§</sup>, H.A. Tanaka<sup>4,‡</sup>, M.M. Tanaka<sup>14,†</sup>, D. Terhorst<sup>42</sup>,  
R. Terri<sup>39</sup>, L.F. Thompson<sup>43</sup>, A. Thorley<sup>27</sup>, S. Tobayama<sup>4</sup>, W. Toki<sup>8</sup>, T. Tomura<sup>47</sup>,  
Y. Totsuka<sup>††</sup>, C. Touramanis<sup>27</sup>, T. Tsukamoto<sup>14,†</sup>, M. Tzanov<sup>28</sup>, Y. Uchida<sup>17</sup>,  
A. Vacheret<sup>36</sup>, M. Vagins<sup>23,5</sup>, G. Vasseur<sup>6</sup>, T. Wachala<sup>13</sup>, A.V. Waldron<sup>36</sup>,  
K. Wakamatsu<sup>35</sup>, C.W. Walter<sup>9,§</sup>, D. Wark<sup>45,36</sup>, W. Warzycha<sup>53</sup>, M.O. Wascko<sup>17</sup>,  
A. Weber<sup>45,36</sup>, R. Wendell<sup>47,§</sup>, R.J. Wilkes<sup>56</sup>, M.J. Wilking<sup>33</sup>, C. Wilkinson<sup>43</sup>,  
Z. Williamson<sup>36</sup>, J.R. Wilson<sup>39</sup>, R.J. Wilson<sup>8</sup>, T. Wongjirad<sup>9</sup>, Y. Yamada<sup>14,†</sup>,  
K. Yamamoto<sup>35</sup>, C. Yanagisawa<sup>33,‡‡</sup>, T. Yano<sup>24</sup>, S. Yen<sup>51</sup>, N. Yershov<sup>22</sup>,  
M. Yokoyama<sup>46,§</sup>, K. Yoshida<sup>25</sup>, T. Yuan<sup>7</sup>, M. Yu<sup>59</sup>, A. Zalewska<sup>13</sup>, J. Zalipska<sup>32</sup>,  
L. Zambelli<sup>14,†</sup>, K. Zaremba<sup>54</sup>, M. Ziembicki<sup>54</sup>, E.D. Zimmerman<sup>7</sup>, M. Zito<sup>6</sup>,  
J. Żmuda<sup>58</sup>

(The T2K Collaboration)

<sup>1</sup>University of Alberta, Centre for Particle Physics, Department of Physics, Edmonton, Alberta, Canada

<sup>2</sup>University of Bern, Albert Einstein Center for Fundamental Physics, Laboratory for High Energy Physics (LHEP), Bern, Switzerland

<sup>3</sup>Boston University, Department of Physics, Boston, Massachusetts, U.S.A.

<sup>4</sup>University of British Columbia, Department of Physics and Astronomy, Vancouver, British Columbia, Canada

<sup>5</sup>University of California, Irvine, Department of Physics and Astronomy, Irvine, California, U.S.A.

<sup>6</sup>IRFU, CEA Saclay, Gif-sur-Yvette, France

<sup>7</sup>University of Colorado at Boulder, Department of Physics, Boulder, Colorado, U.S.A.

<sup>8</sup>Colorado State University, Department of Physics, Fort Collins, Colorado, U.S.A.

<sup>9</sup>Duke University, Department of Physics, Durham, North Carolina, U.S.A.

<sup>10</sup>Ecole Polytechnique, IN2P3-CNRS, Laboratoire Leprince-Ringuet, Palaiseau, France

<sup>11</sup>ETH Zurich, Institute for Particle Physics, Zurich, Switzerland

<sup>12</sup>University of Geneva, Section de Physique, DPNC, Geneva, Switzerland

<sup>13</sup>H. Niewodniczanski Institute of Nuclear Physics PAN, Cracow, Poland

<sup>14</sup>High Energy Accelerator Research Organization (KEK), Tsukuba, Ibaraki, Japan

<sup>15</sup>Institut de Fisica d'Altes Energies (IFAE), Bellaterra (Barcelona), Spain

<sup>16</sup>IFIC (CSIC & University of Valencia), Valencia, Spain

<sup>17</sup>Imperial College London, Department of Physics, London, United Kingdom

<sup>18</sup>INFN Sezione di Bari and Università e Politecnico di Bari, Dipartimento Interuniversitario di Fisica, Bari, Italy

<sup>19</sup>INFN Sezione di Napoli and Università di Napoli, Dipartimento di Fisica, Napoli, Italy

<sup>20</sup>INFN Sezione di Padova and Università di Padova, Dipartimento di Fisica, Padova, Italy

<sup>21</sup>INFN Sezione di Roma and Università di Roma "La Sapienza", Roma, Italy

<sup>22</sup>Institute for Nuclear Research of the Russian Academy of Sciences, Moscow, Russia

<sup>23</sup>Kavli Institute for the Physics and Mathematics of the Universe (WPI), Todai Institutes for Advanced Study, University of Tokyo, Kashiwa, Chiba, Japan

- <sup>24</sup> *Kobe University, Kobe, Japan*
- <sup>25</sup> *Kyoto University, Department of Physics, Kyoto, Japan*
- <sup>26</sup> *Lancaster University, Physics Department, Lancaster, United Kingdom*
- <sup>27</sup> *University of Liverpool, Department of Physics, Liverpool, United Kingdom*
- <sup>28</sup> *Louisiana State University, Department of Physics and Astronomy, Baton Rouge, Louisiana, U.S.A.*
- <sup>29</sup> *Université de Lyon, Université Claude Bernard Lyon 1, IPN Lyon (IN2P3), Villeurbanne, France*
- <sup>30</sup> *Michigan State University, Department of Physics and Astronomy, East Lansing, Michigan, U.S.A.*
- <sup>31</sup> *Miyagi University of Education, Department of Physics, Sendai, Japan*
- <sup>32</sup> *National Centre for Nuclear Research, Warsaw, Poland*
- <sup>33</sup> *State University of New York at Stony Brook, Department of Physics and Astronomy, Stony Brook, New York, U.S.A.*
- <sup>34</sup> *Okayama University, Department of Physics, Okayama, Japan*
- <sup>35</sup> *Osaka City University, Department of Physics, Osaka, Japan*
- <sup>36</sup> *Oxford University, Department of Physics, Oxford, United Kingdom*
- <sup>37</sup> *UPMC, Université Paris Diderot, CNRS/IN2P3, Laboratoire de Physique Nucléaire et de Hautes Energies (LPNHE), Paris, France*
- <sup>38</sup> *University of Pittsburgh, Department of Physics and Astronomy, Pittsburgh, Pennsylvania, U.S.A.*
- <sup>39</sup> *Queen Mary University of London, School of Physics and Astronomy, London, United Kingdom*
- <sup>40</sup> *University of Regina, Department of Physics, Regina, Saskatchewan, Canada*
- <sup>41</sup> *University of Rochester, Department of Physics and Astronomy, Rochester, New York, U.S.A.*
- <sup>42</sup> *RWTH Aachen University, III. Physikalisches Institut, Aachen, Germany*
- <sup>43</sup> *University of Sheffield, Department of Physics and Astronomy, Sheffield, United Kingdom*
- <sup>44</sup> *University of Silesia, Institute of Physics, Katowice, Poland*
- <sup>45</sup> *STFC, Rutherford Appleton Laboratory, Harwell Oxford, and Daresbury Laboratory, Warrington, United Kingdom*
- <sup>46</sup> *University of Tokyo, Department of Physics, Tokyo, Japan*
- <sup>47</sup> *University of Tokyo, Institute for Cosmic Ray Research, Kamioka Observatory, Kamioka, Japan*
- <sup>48</sup> *University of Tokyo, Institute for Cosmic Ray Research, Research Center for Cosmic Neutrinos, Kashiwa, Japan*
- <sup>49</sup> *Tokyo Metropolitan University, Department of Physics, Tokyo, Japan*
- <sup>50</sup> *University of Toronto, Department of Physics, Toronto, Ontario, Canada*
- <sup>51</sup> *TRIUMF, Vancouver, British Columbia, Canada*
- <sup>52</sup> *University of Victoria, Department of Physics and Astronomy, Victoria, British Columbia, Canada*
- <sup>53</sup> *University of Warsaw, Faculty of Physics, Warsaw, Poland*
- <sup>54</sup> *Warsaw University of Technology, Institute of Radioelectronics, Warsaw, Poland*
- <sup>55</sup> *University of Warwick, Department of Physics, Coventry, United Kingdom*
- <sup>56</sup> *University of Washington, Department of Physics, Seattle, Washington, U.S.A.*
- <sup>57</sup> *University of Winnipeg, Department of Physics, Winnipeg, Manitoba, Canada*
- <sup>58</sup> *Wroclaw University, Faculty of Physics and Astronomy, Wroclaw, Poland*
- <sup>59</sup> *York University, Department of Physics and Astronomy, Toronto, Ontario, Canada*
- \* *E-mail: ichikawa@scphys.kyoto-u.ac.jp*

.....  
 The observation of the recent electron neutrino appearance in a muon neutrino beam and the high-precision measurement of the mixing angle  $\theta_{13}$  have led to a re-evaluation of the physics potential of the T2K long-baseline neutrino oscillation experiment. Sensitivities are explored for CP violation in neutrinos, non-maximal  $\sin^2 2\theta_{23}$ , the octant of  $\theta_{23}$ , and the mass hierarchy, in addition to the measurements of  $\delta_{CP}$ ,  $\sin^2 \theta_{23}$ , and  $\Delta m_{32}^2$ , for various combinations of  $\nu$ -mode and  $\bar{\nu}$ -mode data-taking.

With an exposure of  $7.8 \times 10^{21}$  protons-on-target, T2K can achieve 1- $\sigma$  resolution of 0.050(0.054) on  $\sin^2 \theta_{23}$  and  $0.040(0.045) \times 10^{-3} \text{ eV}^2$  on  $\Delta m_{32}^2$  for 100%(50%) neutrino beam mode running assuming  $\sin^2 \theta_{23} = 0.5$  and  $\Delta m_{32}^2 = 2.4 \times 10^{-3} \text{ eV}^2$ . T2K will have sensitivity to the CP-violating phase  $\delta_{CP}$  at 90% C.L. or better over a significant range.

For example, if  $\sin^2 2\theta_{23}$  is maximal (i.e.  $\theta_{23}=45^\circ$ ) the range is  $-115^\circ < \delta_{CP} < -60^\circ$  for normal hierarchy and  $+50^\circ < \delta_{CP} < +130^\circ$  for inverted hierarchy. When T2K data is combined with data from the NO $\nu$ A experiment, the region of oscillation parameter space where there is sensitivity to observe a non-zero  $\delta_{CP}$  is substantially increased compared to if each experiment is analyzed alone.

---

<sup>†</sup> also at J-PARC, Tokai, Japan

<sup>‡</sup> also at Institute of Particle Physics, Canada

<sup>§</sup> affiliated member at Kavli IPMU (WPI), the University of Tokyo, Japan

<sup>¶</sup> also at Moscow Institute of Physics and Technology and National Research Nuclear University "MEPhI", Moscow, Russia

<sup>\*\*</sup> also at JINR, Dubna, Russia

<sup>††</sup> deceased

<sup>‡‡</sup> also at BMCC/CUNY, Science Department, New York, New York, U.S.A.

## 1. Introduction

The experimental confirmation of neutrino oscillations, where neutrinos of a particular flavor ( $\nu_e, \nu_\mu, \nu_\tau$ ) can transmute to another flavor, has profound implications for physics. The observation of a zenith-angle-dependent deficit in muon neutrinos produced by high-energy proton interactions in the atmosphere [1] confirmed the neutrino flavor oscillation hypothesis. The “anomalous” solar neutrino flux [2] problem was shown to be due to neutrino oscillation by more precise measurements [3, 4, 5, 6]. Atmospheric neutrino measurements have provided further precision on the disappearance of muon neutrinos [7, 8] and the appearance of tau neutrinos [9]. Taking advantage of nuclear reactors as intense sources, the disappearance of electron antineutrinos has been firmly established using both widely distributed multiple sources at an average distance of 180 km [6] and from specialized detectors placed within  $\sim 2$  km [10, 11, 12]. The development of high-intensity proton accelerators that can produce focused neutrino beams with mean energy from a few hundred MeV to tens of GeV have enabled measurements of the disappearance of muon-neutrinos (and muon antineutrinos) [8, 13, 14] and appearance of electron-neutrinos (and electron antineutrinos) [15, 16, 17, 18] and tau-neutrinos [19] over distances of hundreds of kilometers.

While the early solar and atmospheric oscillation experiments could be described in a two-neutrino framework, recent experiments with diverse neutrino sources support a three-flavor oscillation framework. In this scenario, the three neutrino flavor eigenstates mix with three mass eigenstates ( $\nu_1, \nu_2, \nu_3$ ) through the Pontecorvo-Maki-Nakagawa-Sakata [20] (PMNS) matrix in terms of three mixing angles ( $\theta_{12}, \theta_{23}, \theta_{13}$ ) and one complex phase ( $\delta_{CP}$ ). The probability of neutrino oscillation depends on these parameters, as well as the difference of the squared masses of the mass states ( $\Delta m_{21}^2, \Delta m_{31}^2, \Delta m_{32}^2$ ). Furthermore, there is an explicit dependence on the energy of the neutrino ( $E_\nu$ ) and the distance traveled ( $L$ ) before detection. To date, all the experimental results are well-described within the neutrino oscillation framework as described in Sec. 2.

T2K is a long-baseline neutrino oscillation experiment proposed in 2003 [21] with three main physics goals that were to be achieved with data corresponding to  $7.8 \times 10^{21}$  protons-on-target (POT) from a 30 GeV proton beam:

- search for  $\nu_\mu \rightarrow \nu_e$  appearance and establish that  $\theta_{13} \neq 0$  with a sensitivity down to  $\sin^2 2\theta_{13} \sim 0.008$  (90% C.L.);
- precision measurement of oscillation parameters in  $\nu_\mu$  disappearance with  $\delta(\Delta m_{32}^2) \sim 10^{-4}$  eV<sup>2</sup> and  $\delta(\sin^2 2\theta_{23}) \sim 0.01$ ; and
- search for sterile components in  $\nu_\mu$  disappearance.

The T2K experiment began data taking in 2009 [22] and a major physics goal, the discovery of  $\nu_\mu \rightarrow \nu_e$  appearance, has been realized at  $7.3 \sigma$  level of significance with just 8.4% of the total approved POT [17]. This is the first time an explicit flavor appearance has been observed from another neutrino flavor with significance larger than  $5\sigma$ . This observation opens the door to study CP violation (CPV) in neutrinos as described in Sec. 2. Following this discovery, the primary physics goal for the neutrino physics community has become a detailed investigation of the three-flavor paradigm which requires determination of the CP-violating phase  $\delta_{CP}$ , resolution of the mass hierarchy (MH), precise measurement of  $\theta_{23}$  to determine how close  $\theta_{23}$  is to  $45^\circ$ , and determination of the  $\theta_{23}$  octant, *i.e.*, whether the mixing angle  $\theta_{23}$  is less than or greater than  $45^\circ$ . T2K, along with the NO $\nu$ A [23] experiment

45 that recently began operation, will lead in the determination of these parameters for at least  
46 a decade.

47 This paper provides a comprehensive update of the anticipated sensitivity of the T2K  
48 experiment to the oscillation parameters as given in the original T2K proposal [21], and  
49 includes an investigation of the enhancements from performing combined fits including the  
50 projected NO $\nu$ A sensitivity. It starts with a brief overview of the neutrino oscillation frame-  
51 work in Sec. 2, and a description of the T2K experiment in Sec. 3. Updated T2K sensitivities  
52 are given in Sec. 4, while sensitivities when results from T2K are combined with those from  
53 the NO $\nu$ A experiment are given in Sec. 5. Finally, results of a study of the optimization of  
54 the  $\nu$  and  $\bar{\nu}$  running time for both T2K and NO $\nu$ A are given in Sec. 6.

## 55 2. Neutrino Mixing and Oscillation Framework

56 Three-generation neutrino mixing can be described by a unitary matrix, often referred to  
57 as the PMNS matrix. The weak flavor eigenstates,  $\nu_e$ ,  $\nu_\mu$ , and  $\nu_\tau$  are related to the mass  
58 eigenstates,  $\nu_1$ ,  $\nu_2$ , and  $\nu_3$ , by the unitary mixing matrix  $U$ :

$$\begin{pmatrix} \nu_e \\ \nu_\mu \\ \nu_\tau \end{pmatrix} = \begin{bmatrix} U_{e1} & U_{e2} & U_{e3} \\ U_{\mu1} & U_{\mu2} & U_{\mu3} \\ U_{\tau1} & U_{\tau2} & U_{\tau3} \end{bmatrix} \begin{pmatrix} \nu_1 \\ \nu_2 \\ \nu_3 \end{pmatrix} \quad (1)$$

59 where the matrix is commonly parameterized as

$$U_{PMNS} = \begin{bmatrix} 1 & 0 & 0 \\ 0 & C_{23} & S_{23} \\ 0 & -S_{23} & C_{23} \end{bmatrix} \begin{bmatrix} C_{13} & 0 & S_{13}e^{-i\delta_{CP}} \\ 0 & 1 & 0 \\ -S_{13}e^{+i\delta_{CP}} & 0 & C_{13} \end{bmatrix} \begin{bmatrix} C_{12} & S_{12} & 0 \\ -S_{12} & C_{12} & 0 \\ 0 & 0 & 1 \end{bmatrix} \quad (2)$$

60 with  $C_{ij}$  ( $S_{ij}$ ) representing  $\cos \theta_{ij}$  ( $\sin \theta_{ij}$ ), where  $\theta_{ij}$  is the mixing angle between the genera-  
61 tions  $i$  and  $j$ . There is one irreducible phase,  $\delta_{CP}$ , allowed in a unitary  $3 \times 3$  mixing matrix.<sup>1</sup>  
62 After neutrinos propagate through vacuum, the probability that they will interact via one  
63 of the three flavors will depend on the values of these mixing angles. As neutrinos propagate  
64 through matter, coherent forward scattering of electron-neutrinos causes a change in the  
65 effective neutrino mass that leads to a modification of the oscillation probability. This is the  
66 so-called *matter effect*. Interference between multiple terms in the transition probability can  
67 lead to CP violation in neutrino mixing if the phase  $\delta_{CP}$  is non-zero.

68 For T2K, the neutrino oscillation modes of interest are the  $\nu_\mu \rightarrow \nu_e$  appearance mode and  
69 the  $\nu_\mu$  disappearance mode. The  $\nu_\mu \rightarrow \nu_e$  appearance oscillation probability (to first order  
70 approximation in the matter effect[24]) is given by

$$\begin{aligned} P(\nu_\mu \rightarrow \nu_e) = & 4C_{13}^2 S_{13}^2 S_{23}^2 \sin^2 \Phi_{31} \left(1 + \frac{2a}{\Delta m_{31}^2} (1 - 2S_{13}^2)\right) \\ & + 8C_{13}^2 S_{12} S_{13} S_{23} (C_{12} C_{23} \cos \delta_{CP} - S_{12} S_{13} S_{23}) \cos \Phi_{32} \sin \Phi_{31} \sin \Phi_{21} \\ & - 8C_{13}^2 C_{12} C_{23} S_{12} S_{13} S_{23} \sin \delta_{CP} \sin \Phi_{32} \sin \Phi_{31} \sin \Phi_{21} \\ & + 4S_{12}^2 C_{13}^2 (C_{12}^2 C_{23}^2 + S_{12}^2 S_{23}^2 S_{13}^2 - 2C_{12} C_{23} S_{12} S_{23} S_{13} \cos \delta_{CP}) \sin^2 \Phi_{21} \\ & - 8C_{13}^2 S_{13}^2 S_{23}^2 (1 - 2S_{13}^2) \frac{aL}{4E_\nu} \cos \Phi_{32} \sin \Phi_{31}, \end{aligned} \quad (3)$$

<sup>1</sup>If the neutrino is a Majorana particle, two additional phases are allowed that have no consequences for neutrino oscillations.

71 where  $\Phi_{ji} = \Delta m_{ji}^2 L / 4E_\nu$ . The terms that include  $a \equiv 2\sqrt{2}G_F n_e E_\nu = 7.56 \times 10^{-5} [\text{eV}^2] (\frac{\rho}{[\text{g/cm}^3]}) (\frac{E_\nu}{[\text{GeV}]})$   
72 are a consequence of the matter effect, where  $n_e$  and  $\rho$  are the electron and matter densities,  
73 respectively. The equivalent expression for antineutrino appearance,  $\bar{\nu}_\mu \rightarrow \bar{\nu}_e$ , is obtained by  
74 reversing the signs of terms proportional to  $\sin \delta_{CP}$  and  $a$ . The first and fourth terms of  
75 Eq.3 come from oscillations induced by  $\theta_{13}$  and  $\theta_{12}$ , respectively, in the presence of non-zero  
76  $\theta_{23}$ . The second and third terms come from interference caused by these oscillations. At the  
77 T2K peak energy of  $\sim 0.6$  GeV and baseline length of  $L = 295$  km,  $\cos \Phi_{32}$  is nearly zero and  
78 the second and fifth terms vanish. The fourth term, to which solar neutrino disappearance  
79 is attributed, is negligibly small. Hence, the dominant contribution for  $\nu_e$  appearance in the  
80 T2K experiment comes from the first and third terms. The contribution from the matter  
81 effect is about 10% of the first term without the matter effect. Since the third term contains  
82  $\sin \delta_{CP}$ , it is called the ‘CP-violating’ term. It is as large as 27% of the first term without the  
83 matter effect when  $\sin \delta_{CP} = 1$  and  $\sin^2 2\theta_{23} = 1$ , meaning that the CP-violating term makes  
84 a non-negligible contribution to the total  $\nu_e$  appearance probability. The measurement of  
85  $\theta_{13}$  from the reactor experiments is independent of the CP phase, and future measurements  
86 from Daya Bay [10], Double Chooz [11] and RENO [12] will reduce the  $\theta_{13}$  uncertainty such  
87 that the significance of the CP-violating term will be enhanced for T2K. It is also impor-  
88 tant to recognize that since the sign of the CP-violating term is opposite for neutrino and  
89 antineutrino oscillations, data taken by T2K with an antineutrino beam for comparison to  
90 neutrino data may allow us to study CP violation effects directly.

91 The  $\nu_\mu$  disappearance oscillation probability is given by

$$1 - P(\nu_\mu \rightarrow \nu_\mu) = (C_{13}^4 \sin^2 2\theta_{23} + S_{23}^2 \sin^2 2\theta_{13}) \sin^2 \Phi_{32} \quad (4)$$

92 (where other matter effect and  $\Delta m_{21}^2$  terms can be neglected). The  $\nu_\mu$  disappearance mea-  
93 surement is sensitive to  $\sin^2 2\theta_{23}$  and  $\Delta m_{32}^2$ . Currently, the measured value of  $\sin^2 2\theta_{23}$  is  
94 consistent with full mixing, but more data are required to know if that is the case. If the  
95 mixing is not maximal, the  $\nu_e$  appearance data, together with the  $\nu_\mu$  disappearance data,  
96 have the potential to resolve the  $\theta_{23}$  octant degeneracy because the first term of Eq.3 is  
97 proportional to  $\sin^2 \theta_{23}$ .

98 The NO $\nu$ A experiment is similar to T2K in the basic goals to measure  $\nu_\mu$  disappearance and  
99  $\nu_e$  appearance in an off-axis muon neutrino beam. The most important difference between  
100 the two experiments is the distance from the neutrino source to the far detector, 810 km for  
101 NO $\nu$ A and 295 km for T2K, with a correspondingly higher peak neutrino beam energy for  
102 NO $\nu$ A to maximize the appearance probability. NO $\nu$ A is projected to have similar sensitivity  
103 compared to T2K for  $\theta_{23}$ ,  $\theta_{13}$ , and  $\delta_{CP}$ , but better sensitivity to the sign of  $\Delta m_{32}^2$  since, as  
104 can be seen in  $a$  in Eq. 3, the size of the matter effect is proportional to the distance  $L$ . The  
105 combination of results from the two experiments at different baselines will further improve  
106 the sensitivity to the sign of  $\Delta m_{32}^2$  and to  $\delta_{CP}$ .

107 In this paper we present the updated T2K sensitivity to neutrino oscillation parameters  
108 using a large value of  $\sin^2 2\theta_{13}$  similar to that measured by the reactor experiments, together  
109 with the sensitivity when projected T2K and NO $\nu$ A results are combined.

110 The latest measured values of the neutrino mixing parameters ( $\theta_{12}$ ,  $\theta_{23}$ ,  $\theta_{13}$ ,  $|\Delta m_{32}^2|$ ,  $\Delta m_{21}^2$ ,  
111  $\delta_{CP}$ ) are listed in Table 1 [25]. The CP-violating phase,  $\delta_{CP}$ , is not yet well constrained,  
112 nor is the sign of  $\Delta m_{32}^2 \equiv m_3^2 - m_2^2$  known. The sign of  $\Delta m_{32}^2$  is related to the ordering of  
113 the three mass eigenstates; the positive sign is referred to as the normal MH (NH) and the

114 negative sign as the inverted MH (IH). Of the mixing angles, the angle  $\theta_{23}$  is measured with  
 115 the least precision; the value of  $\sin^2 2\theta_{23}$  in Table 1 corresponds to  $0.4 < \sin^2(\theta_{23}) < 0.6$ .  
 116 Many theoretical models, e.g. some based on flavor symmetries and some on random draws  
 117 on parameter spaces, sometimes try to explain the origin of the PMNS matrix together  
 118 with the Cabibbo-Kobayashi-Maskawa matrix, which describes mixing in the quark sector.  
 119 Precise determination of how close this mixing angle is to  $45^\circ$  would be an important piece  
 of understanding the origin of flavor mixing of both quarks and leptons.

Table 1: Neutrino oscillation parameters from [25].

Parameter	Value
$\sin^2 2\theta_{12}$	$0.857 \pm 0.024$
$\sin^2 2\theta_{23}$	$> 0.95$
$\sin^2 2\theta_{13}$	$0.095 \pm 0.010$
$\Delta m_{21}^2$	$(7.5 \pm 0.20) \times 10^{-5} \text{ eV}^2$
$ \Delta m_{32}^2 $	$(2.32_{-0.08}^{+0.12}) \times 10^{-3} \text{ eV}^2$
$\delta_{CP}$	unknown

120

### 121 3. T2K Experiment

122 The T2K experiment [22] uses a 30-GeV proton beam accelerated by the J-PARC accelerator  
 123 facility. This is composed of (1) the muon neutrino beamline, (2) the near detector complex,  
 124 which is located 280 m downstream of the neutrino production target, monitors the beam,  
 125 and constrains the neutrino flux parameterization and cross sections, and (3) the far detector,  
 126 Super-Kamiokande (Super-K), which detects neutrinos at a baseline distance of 295 km from  
 127 the target. The neutrino beam is directed  $2.5^\circ$  away from Super-K, producing a narrow-band  
 128  $\nu_\mu$  beam [26] at the far detector. The off-axis angle is chosen such that the energy peaks  
 129 at  $E_\nu = \Delta m_{32}^2 L / 2\pi \approx 0.6 \text{ GeV}$ , which corresponds to the first oscillation minimum of the  $\nu_\mu$   
 130 survival probability at Super-K. This enhances the sensitivity to  $\theta_{13}$  and  $\theta_{23}$  and reduces  
 131 backgrounds from higher-energy neutrino interactions at Super-K.

132 The J-PARC main ring accelerator provides a fast-extracted high-intensity proton beam  
 133 to a graphite target located in the first of three consecutive electro-magnetic horns. Pions  
 134 and kaons produced in the target are focused by the horns and decay in flight to muons and  
 135  $\nu_\mu$ 's in the helium-filled 96-m-long decay tunnel. This is followed by a beam dump and a  
 136 set of muon monitors, which are used to monitor the direction and stability of the neutrino  
 137 beam.

138 The near detector complex contains an on-axis Interactive Neutrino Grid detector  
 139 (INGRID) [27] and an off-axis magnetized detector, ND280. INGRID measures the neu-  
 140 trino interaction event rate at various positions from  $0^\circ$  to  $\sim 1^\circ$  around the beam axis, and  
 141 provides monitoring of the intensity, direction, profile, and stability of the neutrino beam.  
 142 The ND280 off-axis detector measures neutrino beam properties and neutrino interactions  
 143 at approximately the same off-axis angle as Super-K. It is enclosed in a 0.2-T magnet that  
 144 contains a subdetector optimized to measure  $\pi^0$ s (P $\odot$ D) [28], three time projection cham-  
 145 bers (TPC1,2,3) [29] alternating with two one-ton fine-grained detectors (FGD1,2) [30], and



146 an electromagnetic calorimeter (ECal) that surrounds the TPC, FGD, and PØD detectors.  
 147 A side muon range detector (SMRD) [31] built into slots in the magnet return-yoke steel  
 148 detects muons that exit or stop in the magnet steel. A schematic diagram of the detector  
 149 layout has been published elsewhere [22].

150 The Super-K water Cherenkov far detector [32] has a fiducial mass of 22.5 kt contained  
 151 within a cylindrical inner detector (ID) instrumented with 11,129 inward facing 20-inch  
 152 phototubes. Surrounding the ID is a 2-meter wide outer detector (OD) with 1,885 outward-  
 153 facing 8-inch phototubes. A Global Positioning System receiver with <150 ns precision  
 154 synchronizes the timing between reconstructed Super-K events and the J-PARC beam spill.

155 T2K employs various analysis methods to estimate oscillation parameters from the data,  
 156 but in general it is done by comparing the observed and predicted  $\nu_e$  and  $\nu_\mu$  interaction  
 157 rates and energy spectra at the far detector. The rate and spectrum depend on the oscil-  
 158 lation parameters, the incident neutrino flux, neutrino interaction cross sections, and the  
 159 detector response. The initial estimate of the neutrino flux is determined from detailed sim-  
 160 ulations incorporating proton beam measurements, INGRID measurements, and pion and  
 161 kaon production measurements from the NA61/SHINE [33, 34] experiment. The ND280  
 162 detector measurement of  $\nu_\mu$  charged current (CC) events is used to constrain the initial flux  
 163 estimates and parameters of the neutrino interaction models that affect the predicted rate  
 164 and spectrum of neutrino interactions at both ND280 and Super-K. At Super-K,  $\nu_e$  and  $\nu_\mu$   
 165 charged current quasi-elastic (CCQE) events, for which the neutrino energy can be recon-  
 166 structed using simple kinematics, are selected. Efficiencies and backgrounds are determined  
 167 through detailed simulations tuned to control samples which account for final state inter-  
 168 actions (FSI) inside the nucleus and secondary hadronic interactions (SI) in the detector  
 169 material. These combined results are used in a fit to determine the oscillation parameters.

170 As of May 2013, T2K has accumulated  $6.57 \times 10^{20}$  POT, which corresponds to about 8.4%  
 171 of the total approved data. Results from this dataset on the measurement of  $\theta_{23}$  and  $|\Delta m_{32}^2|$   
 172 by  $\nu_\mu$  disappearance [14], and of  $\theta_{13}$  and  $\delta_{CP}$  by  $\nu_e$  appearance have been published [17]. It  
 173 is reported in [17] that combining the T2K result with the world average value of  $\theta_{13}$  from  
 174 reactor experiments leads to some values of  $\delta_{CP}$  being disfavored at 90% CL.

#### 175 4. T2K Projected Sensitivities to Neutrino Oscillation Parameters

176 To demonstrate the T2K physics potential, we have performed sensitivity studies using  
 177 combined fits to the reconstructed energy spectra of  $\nu_e(\bar{\nu}_e)$  and  $\nu_\mu(\bar{\nu}_\mu)$  events observed  
 178 at Super-K with both  $\nu$ -mode beam, and  $\bar{\nu}$ -mode beam in the three-flavor mixing model.  
 179 Results shown here generally use the systematic errors established for the 2012 oscillation  
 180 analyses [35, 16] as described below, although, in addition, we have studied cases with  
 181 projected systematic errors as described in Sec. 4.5.

182 Since the sensitivity depends on the true values of the oscillation parameters, a set of  
 183 oscillation parameters ( $\theta$ ) is chosen as a test point for each study and is used to generate  
 184 simulated ‘observed’ reconstructed energy spectra. Then, a hypothesis test for the set of  
 185 parameters of interest ( $H_0$ ) is applied using

$$\Delta\chi^2 = \chi^2(H_0) - \chi_{min}^2. \quad (5)$$

186 The value of  $\chi^2(H_0)$  is calculated as  $-2 \ln \mathcal{L}(\theta|H_0)$ , where  $\mathcal{L}(\theta|H_0)$  is the likelihood to observe  
 187 the spectrum generated at  $\theta$  when the ‘true’ oscillation parameters are given by  $H_0$ . The

188 minimum value of  $\chi^2$  in the oscillation parameter space is given by  $\chi_{min}^2$ . The oscillation  
 189 parameter set which gives  $\chi_{min}^2$  is equivalent to  $\theta$ , since spectra are generated without statis-  
 190 tical fluctuations in this analysis. When we test only one or two of the five varied oscillation  
 191 parameters ( $\sin^2 2\theta_{13}$ ,  $\delta_{CP}$ ,  $\sin^2 \theta_{23}$ ,  $\Delta m_{32}^2$ , and the MH), the tested parameters are fixed  
 192 at a set of test points, and the remaining oscillation parameters are fit to give a minimized  
 193  $\chi^2(H_0)$ .

194 In most cases, this  $\Delta\chi^2$  closely resembles a  $\chi^2$  distribution for  $n$  degrees of freedom,  
 195 where  $n$  corresponds to the number of tested oscillation parameters. Then, critical  $\chi^2$  values  
 196 for Gaussian distributed variables ( $\Delta\chi_{critical}^2$ ) can be used for determining confidence level  
 197 (C.L.) regions [36]. Each simulated spectrum is generated at the MC sample statistical mean,  
 198 and therefore the results of this test represent the median sensitivity. Thus the results of  
 199 these studies indicate that half of experiments are expected to be able to reject  $H_0$  at the  
 200 reported C.L. This is accurate if two conditions are met: (1) the probability density function  
 201 (pdf) for  $\Delta\chi^2$  follows a true  $\chi^2$  distribution, and (2) the  $\Delta\chi^2$  value calculated with the MC  
 202 sample statistical mean spectra ( $\Delta\bar{\chi}^2$ ) is equivalent to the median of the  $\Delta\chi^2$  pdf. Then,  
 203  $\Delta\bar{\chi}^2$  can be used to construct median sensitivity C.L. contours. Studies using ensembles of  
 204 toy MC experiments where statistical fluctuations expected at a given POT and systematic  
 205 fluctuations are included have shown that calculating C.L.s by applying a  $\Delta\chi_{critical}^2$  value  
 206 to  $\Delta\chi^2$  gives fairly consistent C.L.s, and that  $\Delta\bar{\chi}^2$  is in good agreement with the median  
 207  $\Delta\chi^2$  value of each ensemble of toy MC experiments, except in the case of a mass hierarchy  
 208 determination. Therefore, in this paper we show C.L.s constructed by applying the  $\Delta\chi_{critical}^2$   
 209 value to  $\Delta\bar{\chi}^2$  as our median sensitivity. The exception of the MH case will be discussed in  
 210 detail in Sec. 5.

#### 211 4.1. *Expected observables and summary of current systematic errors*

212 Our sensitivity studies are based on the signal efficiency, background, and systematic errors  
 213 established for the T2K 2012 oscillation analyses[35, 16]; however, we note that errors are  
 214 lower in more recent published analyses. Since official T2K systematic errors are used, these  
 215 errors have been reliably estimated based on data analysis, unlike previous sensitivity studies  
 216 which use errors based only on simulation and estimations [21]. Systematic errors therefore  
 217 include both normalization and shape errors, and are implemented as a covariance matrix  
 218 for these studies, where full correlation between  $\nu$ - and  $\bar{\nu}$ -modes is generally assumed.

219 For the  $\nu_e$  sample, interaction candidate events fully contained in the fiducial volume with  
 220 a single electron-like Cherenkov ring are selected. The visible energy is required to exceed  
 221 100 MeV/c, events with a delayed electron signal are rejected, and events with an invariant  
 222 mass near that of the  $\pi^0$  are rejected, where the invariant mass is reconstructed assuming  
 223 the existence of a second ring. Finally, events are required to have a reconstructed neutrino  
 224 energy below 1250 MeV. The efficiency of the event selection for the CC  $\nu_e$  signal is 62%  
 225 and the fraction of CCQE events in the signal is 80%. For the  $\nu_\mu$  sample, again events  
 226 must be fully contained in the fiducial volume, but they must now have a single muon-like  
 227 Cherenkov ring with a momentum exceeding 200 MeV/c. There must be either zero or one  
 228 delayed electron. The efficiency and purity of  $\nu_\mu$  CCQE events are estimated to be 72% and  
 229 61%, respectively.

230 Fits are performed by calculating  $\Delta\chi^2$  using a binned likelihood method for the appearance  
 231 and disappearance reconstructed energy spectra in Super-K. Reconstructed appearance and  
 232 disappearance energy spectra generated for the approved full T2K statistics,  $7.8 \times 10^{21}$  POT,  
 233 assuming a data-taking condition of either 100%  $\nu$ -mode or 100%  $\bar{\nu}$ -mode are given in Fig.  
 234 1. These spectra are generated assuming the nominal oscillation parameters given in Table  
 235 3.

236 Although errors on the shape of the reconstructed energy spectra are used for the analysis  
 237 described in Sec. 4, the total error on the number of events at Super-K is given in Table 2.  
 238 This includes uncertainties on the flux prediction, uncertainties on  $\nu$  interactions both con-  
 239 strained by the near detector and measured by external experiments, Super-K detector  
 240 errors, and final state interaction uncertainties, all of which can cause fluctuations in the  
 241 shape of the final reconstructed energy spectra.

Table 2: The systematic errors in percentage on the predicted number of events at Super-K (assuming the oscillation parameters given in Table 3 are the true values of the oscillation parameters) as used in the 2012 oscillation analyses.

	Appearance	Disappearance
Flux and cross section constrained by the near detector	5.0 %	4.2 %
Cross section not constrained by the near detector	7.4 %	6.2 %
Super-K detector and FSI	3.9 %	11.0 %
Total	9.7 %	13.3 %

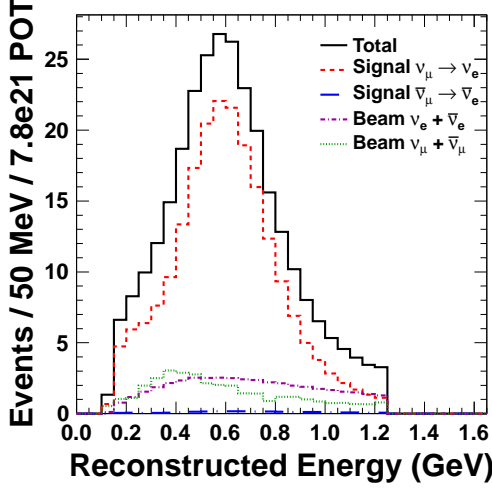
242 When performing fits, the oscillation parameters  $\delta_{CP}$ ,  $\sin^2 2\theta_{13}$ ,  $\sin^2 \theta_{23}$ , and  $\Delta m_{32}^2$  are  
 243 considered unknown unless otherwise stated, while  $\sin^2 2\theta_{12}$  and  $\Delta m_{21}^2$  are assumed fixed  
 244 to the values given in this table. Tables 4 and 5 give the number of events expected with  
 245 the T2K full statistics. Fig. 2 shows the dependence of the  $\nu_e$  appearance reconstructed  
 246 energy spectrum on  $\delta_{CP}$ . Some of the sensitivities are enhanced by constraining the error  
 247 on  $\sin^2 2\theta_{13}$  based on the projected precision of reactor measurements. For this study, the  
 248 uncertainty (referred to as the ultimate reactor error) on  $\sin^2 2\theta_{13}$  is chosen to be 0.005,  
 which corresponds to the 2012 systematic error only of the Daya Bay experiment[37]<sup>2</sup>.

Table 3: Nominal values of the oscillation parameters. When the reactor constraint is used, we assume 0.005 as the expected uncertainty of the reactor measurement.

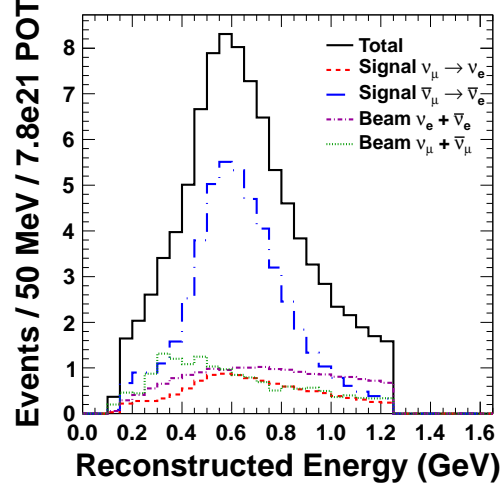
Parameter	$\sin^2 2\theta_{13}$	$\delta_{CP}$	$\sin^2 \theta_{23}$	$\Delta m_{32}^2$	Hierarchy	$\sin^2 2\theta_{12}$	$\Delta m_{21}^2$
Nominal Value	0.1	0	0.5	$2.4 \times 10^{-3}$ eV <sup>2</sup>	normal	0.8704	$7.6 \times 10^{-5}$ eV <sup>2</sup>

249

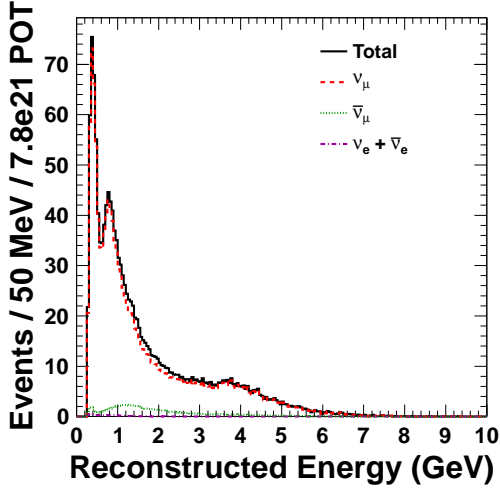
<sup>2</sup>The statistical error is 0.010 for [37]



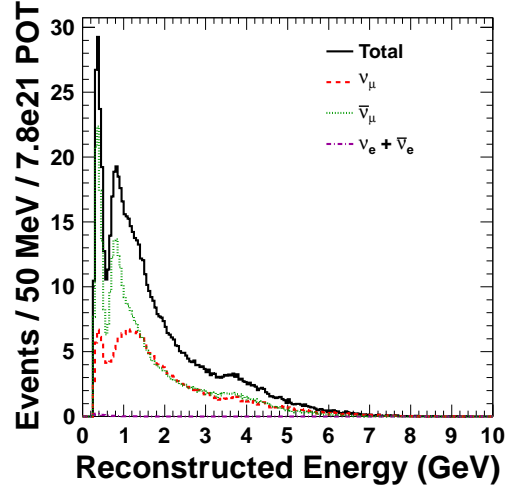
(a)  $\nu_e$  appearance reconstructed energy spectrum, 100%  $\nu$ -mode running.



(b)  $\bar{\nu}_e$  appearance reconstructed energy spectrum, 100%  $\bar{\nu}$ -mode running.



(c)  $\nu_\mu$  disappearance reconstructed energy spectrum, 100%  $\nu$ -mode running.



(d)  $\bar{\nu}_\mu$  disappearance reconstructed energy spectrum, 100%  $\bar{\nu}$ -mode running.

Fig. 1: Appearance and disappearance reconstructed energy spectra in Super-K for  $\nu_e$ ,  $\nu_\mu$ ,  $\bar{\nu}_e$ , and  $\bar{\nu}_\mu$  at  $7.8 \times 10^{21}$  POT for the nominal oscillation parameters as given in Table 3

#### 250 4.2. Expected 90% C.L. regions

251 In this section we show expected 90% C.L. intervals for the T2K full statistics of  $7.8 \times$   
 252  $10^{21}$  POT. Contours showing both the T2K sensitivity for  $\delta_{CP}$  vs.  $\sin^2 2\theta_{13}$  and for  $\Delta m_{32}^2$   
 253 vs.  $\sin^2 \theta_{23}$  are provided, where the assumed true value of the oscillation parameters is  
 254 indicated by a black cross. The oscillation parameters  $\delta_{CP}$ ,  $\sin^2 2\theta_{13}$ ,  $\sin^2 \theta_{23}$ , and  $\Delta m_{32}^2$  are  
 255 considered unknown, as stated above. Both the NH and IH are considered, and  $\Delta\chi^2$  values  
 256 are calculated from the minimum  $\chi^2$  value for both MH assumptions. The blue curves are  
 257 generated assuming the correct MH and the red curves are generated assuming the incorrect  
 258 MH, such that if an experiment or combination of experiments from the global neutrino  
 259 community were to determine the MH the red contour would be eliminated. A contour

Table 4: Expected numbers of  $\nu_e$  or  $\bar{\nu}_e$  appearance events at  $7.8 \times 10^{21}$  POT. The number of events is broken down into those coming from: appearance signal or intrinsic beam background events that undergo charged current (CC) interactions in Super-K, or beam background events that undergo neutral current (NC) interactions.

	$\delta_{CP}$	Total	Signal $\nu_\mu \rightarrow \nu_e$	Signal $\bar{\nu}_\mu \rightarrow \bar{\nu}_e$	Beam CC $\nu_e + \bar{\nu}_e$	Beam CC $\nu_\mu + \bar{\nu}_\mu$	NC
100% $\nu$ -mode	$0^\circ$	291.5	211.9	2.4	41.3	1.4	34.5
100% $\nu$ -mode	$-90^\circ$	341.8	262.9	1.7			
100% $\bar{\nu}$ -mode	$0^\circ$	94.9	11.2	48.8	17.2	0.4	17.3
100% $\bar{\nu}$ -mode	$-90^\circ$	82.9	13.1	34.9			

Table 5: Expected numbers of  $\nu_\mu$  or  $\bar{\nu}_\mu$  disappearance events for  $7.8 \times 10^{21}$  POT. The first two columns show the number of  $\nu_\mu$  and  $\bar{\nu}_\mu$  events, broken down into those that undergo charged-current quasi-elastic (CCQE) scattering at Super-K, and those that undergo other types of CC scattering (CC non-QE). The third column shows CC  $\nu_e$  and  $\bar{\nu}$  events, both from intrinsic beam backgrounds and oscillations, while the fourth column shows NC events.

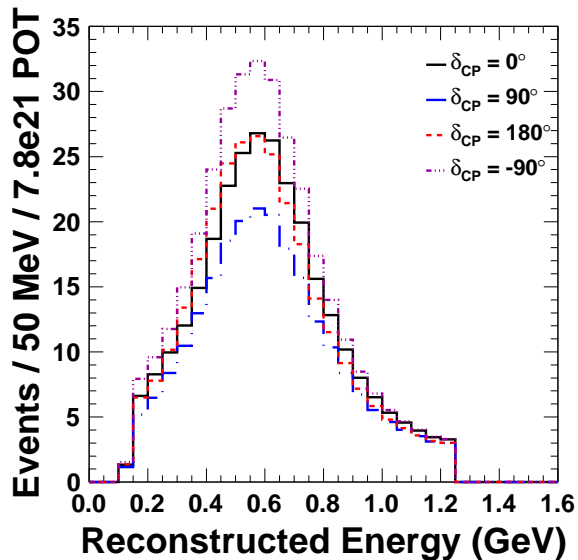
	Total	CCQE $\nu_\mu(\bar{\nu}_\mu)$	CC non-QE $\nu_\mu(\bar{\nu}_\mu)$	CC $\nu_e + \bar{\nu}_e$ CC $\nu_\mu(\bar{\nu}_\mu) \rightarrow \nu_e(\bar{\nu}_e)$	NC
100% running in $\nu$ -mode	1,493	782(48)	544 (40)	4	75
100% running in $\bar{\nu}$ -mode	715	130(263)	151(138)	0.5	33

260 consisting of the outermost edge of all contours in each plot can be considered as the T2K  
 261 sensitivity assuming an unknown MH. For the sake of brevity, only results assuming true  
 262 NH are shown; similar conclusions can be drawn from plots assuming true IH.

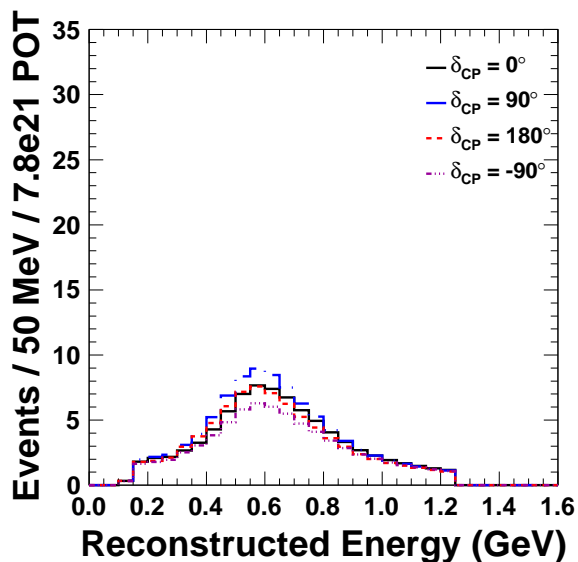
263 Figure 3 gives an example of the difference in the shape of the T2K sensitive region for  $\nu$ -  
 264 vs.  $\bar{\nu}$ -mode at true  $\delta_{CP} = -90^\circ$  (and the other oscillation parameters as given in Table 3)  
 265 by comparing the  $\nu$ -mode – Fig. 3 (a) – and  $\bar{\nu}$ -mode – Fig. 3 (b) – C.L. contours without a  
 266 reactor constraint at 50% of the full T2K POT. These two contours are then combined in  
 267 Fig. 3 (c), which shows the 90% C.L. region for 50%  $\nu$ - plus 50%  $\bar{\nu}$ -mode running to achieve  
 268 the full T2K POT. This demonstrates that  $\delta_{CP}$  can be constrained by combining  $\nu$ -mode  
 269 and  $\bar{\nu}$ -mode data.

270 Figures 4 and 5 show example 90% C.L. regions for  $\delta_{CP}$  vs.  $\sin^2 2\theta_{13}$  at the full T2K  
 271 statistics, both for T2K alone and including an extra constraint on the T2K predicted data  
 272 fit based on the ultimate reactor error  $\delta(\sin^2 2\theta_{13}) = 0.005$  as discussed above, for true  $\delta_{CP}$  of  
 273  $0^\circ$  and  $-90^\circ$ , respectively. In the case of  $\delta_{CP} = -90^\circ$ , we start to have sensitivity to resolve  
 274  $\delta_{CP}$  without degeneracies.

275 Figure 6 shows example 90% C.L. regions for  $\Delta m_{32}^2$  vs.  $\sin^2 \theta_{23}$  at the full T2K statistics  
 276 for  $\sin^2 \theta_{23} = 0.4$ . The  $\theta_{23}$  octant can be resolved in this case by combining both  $\nu$ -mode and  
 277  $\bar{\nu}$ -mode data and also including a reactor constraint on  $\theta_{13}$ , where this combination of inputs  
 278 is required to resolve degeneracies between the oscillation parameters  $\sin^2 \theta_{23}$ ,  $\sin^2 2\theta_{13}$ , and  
 279  $\delta_{CP}$ , demonstrating the importance of the reactor constraint in this case.



(a)  $\nu$ -mode running

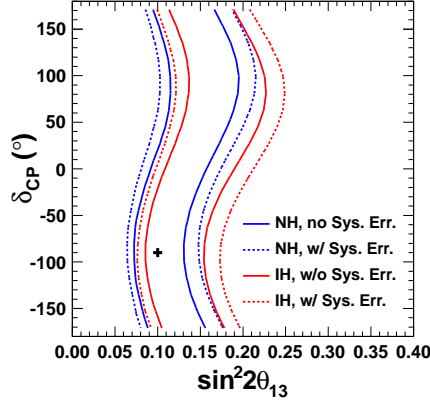


(b)  $\bar{\nu}$ -mode running

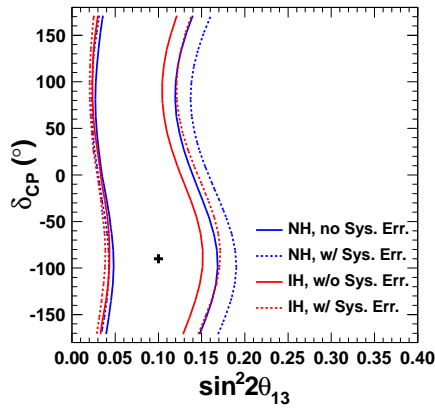
Fig. 2:  $\nu_e$  appearance reconstructed energy spectra in Super-K for  $7.8 \times 10^{21}$  POT in either  $\nu$ -mode or  $\bar{\nu}$ -mode at various values of assumed true  $\delta_{CP}$  with  $\sin^2 \theta_{23} = 0.5$ .

#### 280 4.3. Sensitivities for CP-violating term, non-maximal $\theta_{23}$ , and $\theta_{23}$ octant

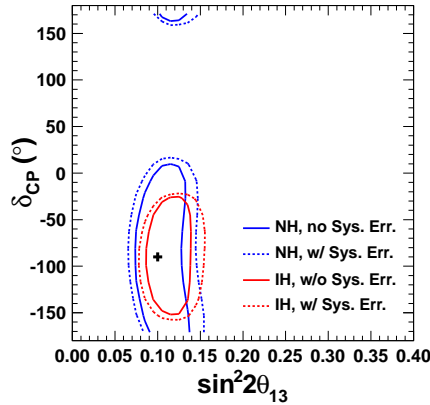
281 The sensitivities for CP violation, non-maximal  $\theta_{23}$ , and the octant of  $\theta_{23}$  (i.e., whether the  
 282 mixing angle  $\theta_{23}$  is less than or greater than  $45^\circ$ ) depend on the true oscillation parameter  
 283 values. Fig. 7 shows the expected  $\Delta\chi^2$  for the  $\sin \delta_{CP} = 0$  hypothesis, for various true values  
 284 of  $\delta_{CP}$  and  $\sin^2 \theta_{23}$ . To see the dependence more clearly,  $\Delta\chi^2$  is plotted as a function of  $\delta_{CP}$   
 285 for various values of  $\sin^2 \theta_{23}$  in Fig. 8 (normal MH case) and Fig. 9 (inverted MH case). For  
 286 favorable sets of the oscillation parameters and mass hierarchy, T2K will have greater than  
 287 90% C.L. sensitivity to non-zero  $\sin \delta_{CP}$ .



(a) 50%  $\nu$ -mode only.



(b) 50%  $\bar{\nu}$ -mode only.



(c) 50%  $\nu$ -, 50%  $\bar{\nu}$ -mode.

Fig. 3: Expected  $\delta_{CP}$  vs.  $\sin^2 2\theta_{13}$  90% C.L. intervals, where (a) and (b) are each given for 50% of the full T2K POT, and (c) demonstrates the sensitivity of the total T2K POT with 50%  $\nu$ -mode plus 50%  $\bar{\nu}$ -mode running. Contours are plotted for the case of true  $\delta_{CP} = -90^\circ$  and NH. The blue curves are fit assuming the correct MH(NH)

, while the red are fit assuming the incorrect MH(IH), and contours are plotted from the minimum  $\chi^2$  value for both MH assumptions. The solid contours are with statistical error only, while the dashed contours include the systematic errors used in the 2012 oscillation analysis assuming full correlation between  $\nu$ - and  $\bar{\nu}$ -mode running errors.

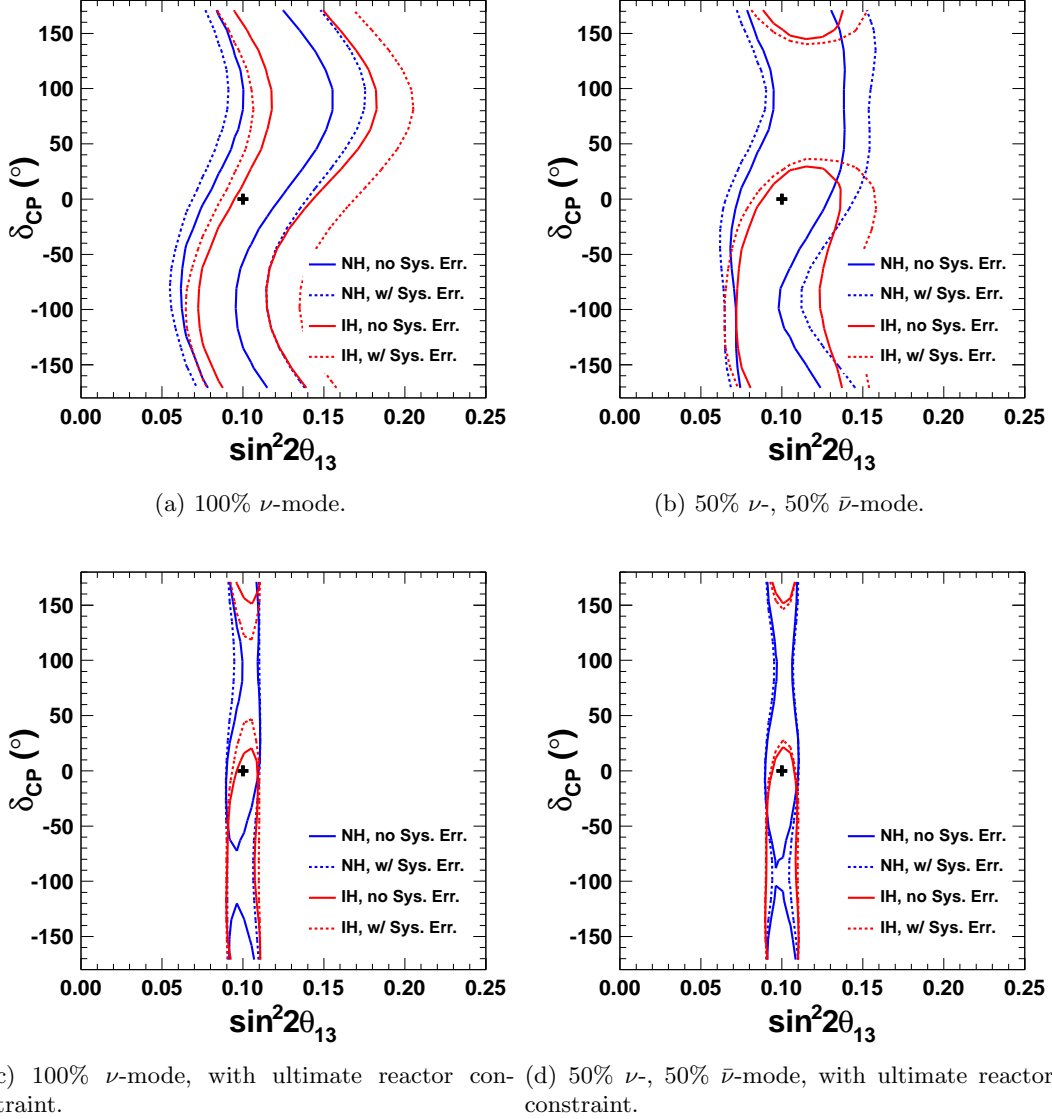


Fig. 4:  $\delta_{CP}$  vs.  $\sin^2 2\theta_{13}$  90% C.L. intervals for  $7.8 \times 10^{21}$  POT. Contours are plotted for the case of true  $\delta_{CP} = 0^\circ$  and NH. The blue curves are fit assuming the correct MH(NH), while the red are fit assuming the incorrect MH(IH), and contours are plotted from the minimum  $\chi^2$  value for both MH assumptions. The solid contours are with statistical error only, while the dashed contours include the 2012 systematic errors fully correlated between  $\nu$ - and  $\bar{\nu}$ -mode.

288 Figures 10 and 11 show the  $\sin^2 \theta_{23}$  vs.  $\delta_{CP}$  regions where T2K has more than a 90% C.L.  
 289 sensitivity to reject maximal mixing or reject one octant of  $\theta_{23}$ . In each of these figures, the  
 290 oscillation parameters  $\delta_{CP}$ ,  $\sin^2 2\theta_{13}$ ,  $\sin^2 \theta_{23}$ ,  $\Delta m_{32}^2$ , and the MH are considered unknown  
 291 and a constraint based on the ultimate reactor error is used. Note that the T2K sensitivity  
 292 to reject maximal mixing is roughly independent of  $\nu - \bar{\nu}$  running ratio, while the sensitivity  
 293 to reject one octant is better when  $\nu$ - and  $\bar{\nu}$ -modes are combined. Again, the combination  
 294 of  $\nu$ - and  $\bar{\nu}$ -modes, as well as the tight constraint on  $\theta_{13}$  from the reactor measurement,



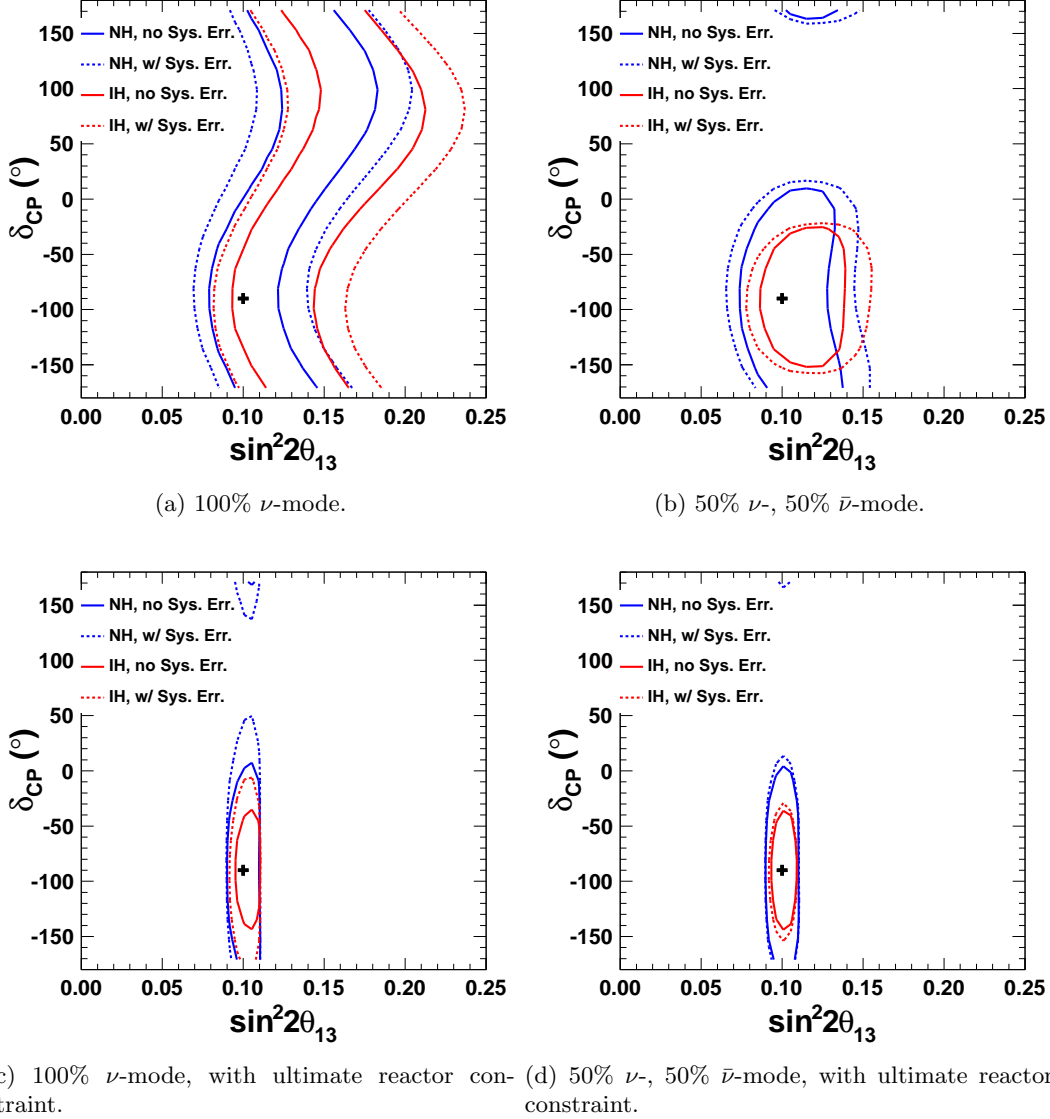


Fig. 5:  $\delta_{CP}$  vs.  $\sin^2 2\theta_{13}$  90% C.L. intervals for  $7.8 \times 10^{21}$  POT. Contours are plotted for the case of true  $\delta_{CP} = -90^\circ$  and NH. The blue curves are fit assuming the correct MH(NH), while the red are fit assuming the incorrect MH(IH), and contours are plotted from the minimum  $\chi^2$  value for both MH assumptions. The solid contours are with statistical error only, while the dashed contours include the 2012 systematic errors fully correlated between  $\nu$ - and  $\bar{\nu}$ -mode.

295 are all required to resolve the correct values for the parameters  $\sin^2 \theta_{23}$ ,  $\sin^2 2\theta_{13}$ , and  $\delta_{CP}$   
 296 from many possible solutions. Resolving the values of these three oscillation parameters is  
 297 required in order to also resolve the  $\theta_{23}$  octant.

298 These figures show that by running with a significant amount of  $\bar{\nu}$ -mode, T2K has sensi-  
 299 tivity to the CP-violating term and octant of  $\theta_{23}$  for a wider region of oscillation parameters  
 300 ( $\delta_{CP}, \theta_{23}$ ) and for both mass hierarchies, particularly when systematic errors are taken into  
 301 account. The optimal running ratio is discussed in more detail in Sec. 6.

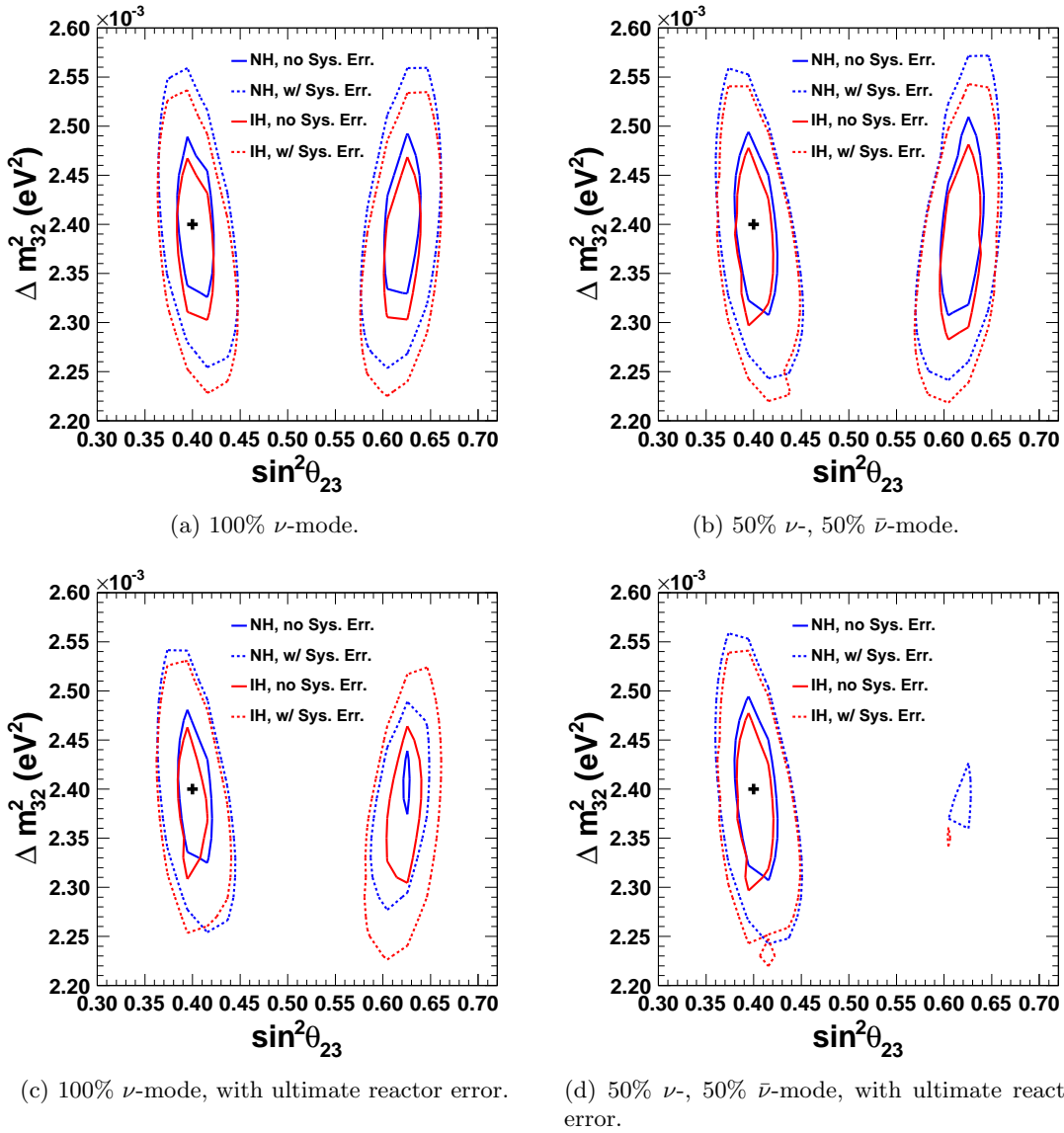


Fig. 6:  $\Delta m_{32}^2$  vs.  $\sin^2 \theta_{23}$  90% C.L. intervals for  $7.8 \times 10^{21}$  POT. Contours are plotted for the case of true  $\delta_{CP} = 0^\circ$ ,  $\sin^2 \theta_{23} = 0.4$ ,  $\Delta m_{32}^2 = 2.4 \times 10^{-3}$  eV<sup>2</sup> and NH. The blue curves are fit assuming the correct MH(NH), while the red are fit assuming the incorrect MH(IH), and contours are plotted from the minimum  $\chi^2$  value for both MH assumptions. The solid contours are with statistical error only, while the dashed contours include the 2012 systematic errors fully correlated between  $\nu$ - and  $\bar{\nu}$ -mode.

#### 302 4.4. Precision or sensitivity vs. POT

303 The T2K uncertainty (i.e. precision) vs. POT for  $\sin^2 \theta_{23}$  and  $\Delta m_{32}^2$  is given in Fig. 12 for the  
 304 100%  $\nu$ -mode running case and the 50% plus 50%  $\nu - \bar{\nu}$ -mode running case. The precision  
 305 includes either statistical errors only, statistical errors combined with the 2012 systematic  
 306 errors, or statistical errors combined with conservatively-projected systematic errors for the  
 307 full POT. See Sec. 4.5 for details about the projected systematic errors used.

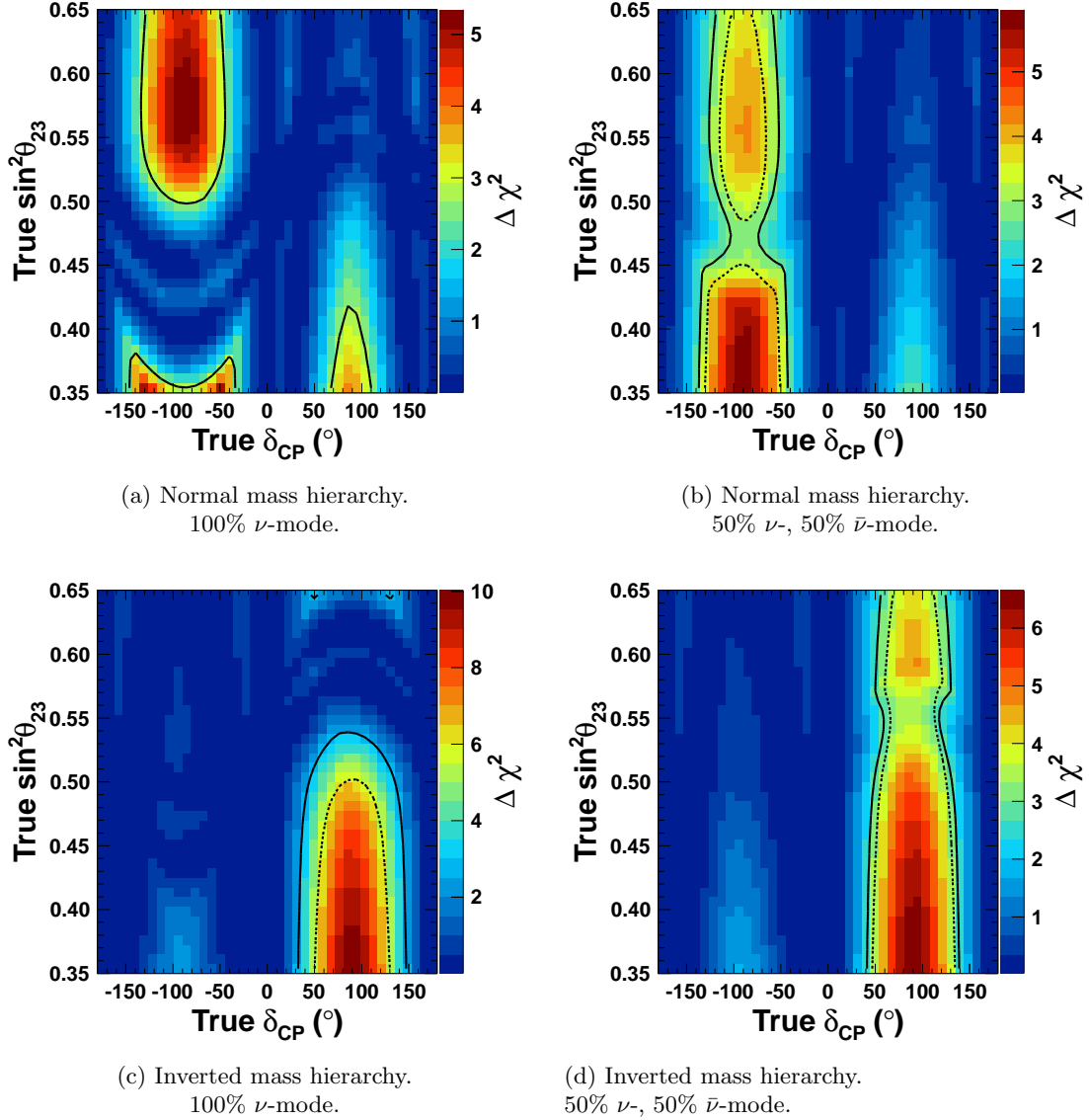


Fig. 7: The expected  $\Delta\chi^2$  for the  $\sin\delta_{CP} = 0$  hypothesis, in the  $\delta_{CP} - \sin^2\theta_{23}$  plane. The  $\Delta\chi^2$  map shown in color is calculated assuming no systematic errors. The solid contours show the 90% C.L. sensitivity with statistical error only, while the dashed contours include the 2012 T2K systematic error. The dashed contour does not appear in (a) because T2K does not have 90% C.L. sensitivity in this case.

308 Generally, the effect of the systematic errors is reduced by running with combined  $\nu$ -mode  
 309 and  $\bar{\nu}$ -mode. When running 50% in  $\nu$ -mode and 50% in  $\bar{\nu}$ -mode, the statistical  $1\sigma$  uncertainty  
 310 of  $\sin^2\theta_{23}$  and  $\Delta m_{32}^2$  is 0.045 and  $0.04 \times 10^{-3} \text{ eV}^2$ , respectively, at the T2K full statistics.

311 It should be noted that the sensitivity to  $\sin^2\theta_{23}$  shown here for the current exposure  
 312 ( $6.57 \times 10^{20}$  POT) is significantly worse than the most recent T2K result [14], and in fact the  
 313 recent result is quite close to the final sensitivity (at  $7.8 \times 10^{21}$  POT) shown. This apparent  
 314 discrepancy comes from three factors. About half of the difference between the expected  
 315 sensitivity and observed result is due to an apparent statistical fluctuation, where fewer T2K

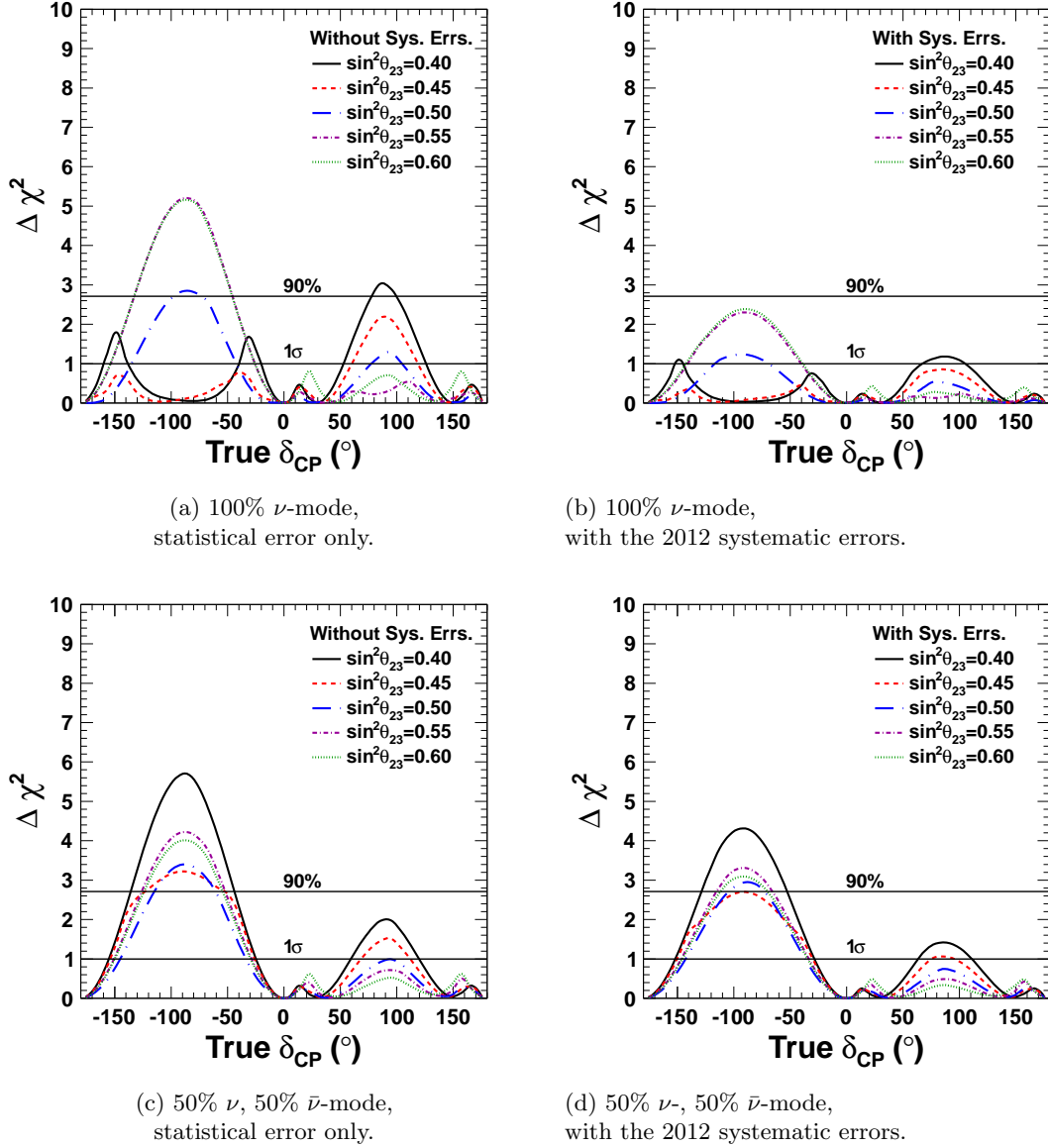
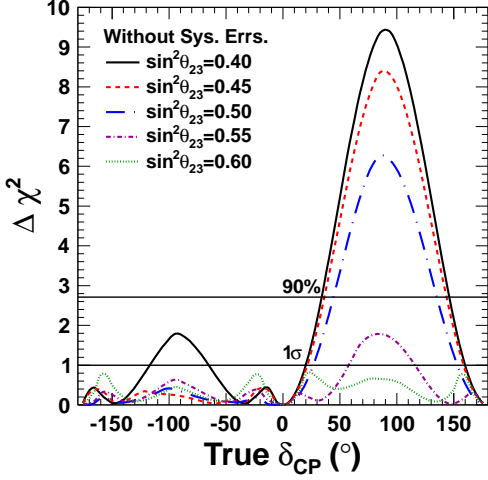
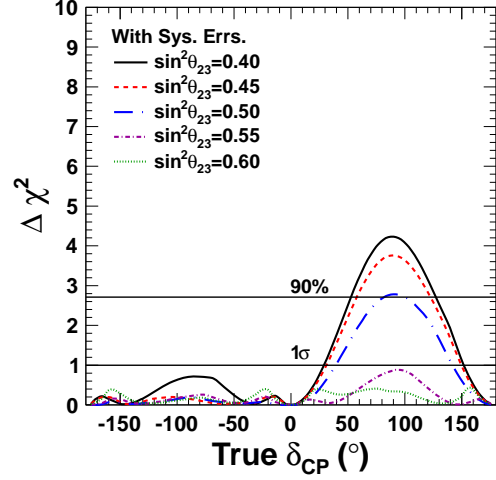


Fig. 8: The expected  $\Delta\chi^2$  for the  $\sin\delta_{CP} = 0$  hypothesis, plotted as a function of  $\delta_{CP}$  for various values of  $\sin^2\theta_{23}$  (given in the legend) in the case of normal mass hierarchy.

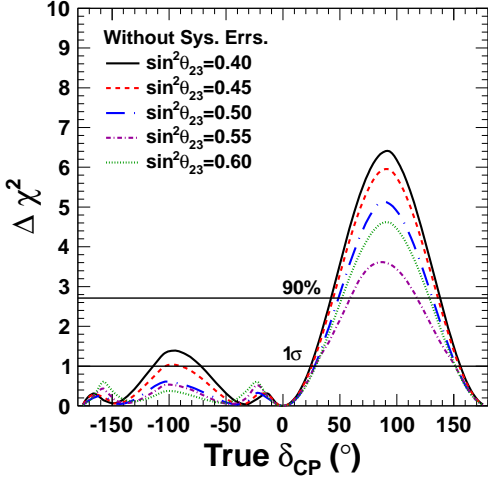
316  $\nu_\mu$  events have been observed than expected. Of the remaining difference, half comes from  
 317 the use of a Feldman-Cousins statistical analysis for the T2K official oscillation result which  
 318 this sensitivity study does not use. The rest comes from the location of the best fit point: the  
 319 expected error depends on the true value of  $\sin^2\theta_{23}$  because a local minimum in each octant  
 320 on each side of the point of maximal disappearance,  $\sin^2\theta_{23} \simeq 0.503$  for  $\sin^2 2\theta_{13} = 0.1$ ,  
 321 increases the full width of the  $\Delta\chi^2$  curve such that the farther the true point is from maximal  
 322 disappearance, the larger the error on  $\sin^2\theta_{23}$  becomes (where the studies here assume a true  
 323 value of  $\sin^2\theta_{23}$  slightly lower than the point of maximal disappearance –  $\sin^2\theta_{23} = 0.5$ ).  
 324 Therefore, if results from future running continue to favor maximal disappearance we expect



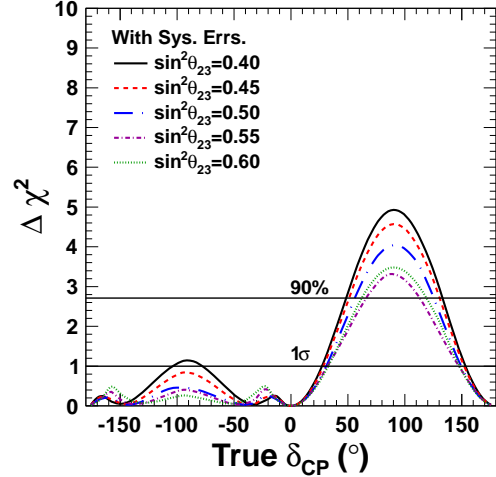
(a) 100%  $\nu$ -mode,  
statistical error only.



(b) 100%  $\nu$ -mode,  
with the 2012 systematic errors.



(c) 50%  $\nu$ , 50%  $\bar{\nu}$ -mode,  
statistical error only.



(d) 50%  $\nu$ , 50%  $\bar{\nu}$ -mode,  
with the 2012 systematic errors.

Fig. 9: The expected  $\Delta\chi^2$  for the  $\sin\delta_{CP} = 0$  hypothesis, plotted as a function of  $\delta_{CP}$  for various values of  $\sin^2\theta_{23}$  (given in the legend) in the case of inverted mass hierarchy.

325 modest improvements in our current constraints, eventually approaching a value close to,  
326 and possibly slightly better than, the predicted final sensitivity shown here.

327 Figure 13 shows the  $\sin^2\theta_{23}$  region where maximal mixing or one of the  $\theta_{23}$  octants can be  
328 rejected, as a function of POT in the case of 50%  $\nu$ - plus 50%  $\bar{\nu}$ -mode running. Although these  
329 plots are made under the condition that the true mass hierarchy is normal and  $\delta_{CP} = 0^\circ$ ,  
330 dependence on these conditions is moderate in the case of 50%  $\nu$ - plus 50%  $\bar{\nu}$ -mode running.

331 The sensitivity to reject the null hypothesis  $\sin\delta_{CP} = 0$  depends on the true oscillation  
332 parameters and is expected to be greatest for the case  $\delta_{CP} = +90^\circ$  and inverted MH.  
333 Figure 14 shows how the expected  $\Delta\chi^2$  evolves as a function of POT in this case, as well as  
334 for  $\delta_{CP} = -90^\circ$  and normal MH, another case in which the sensitivity is high. These plots

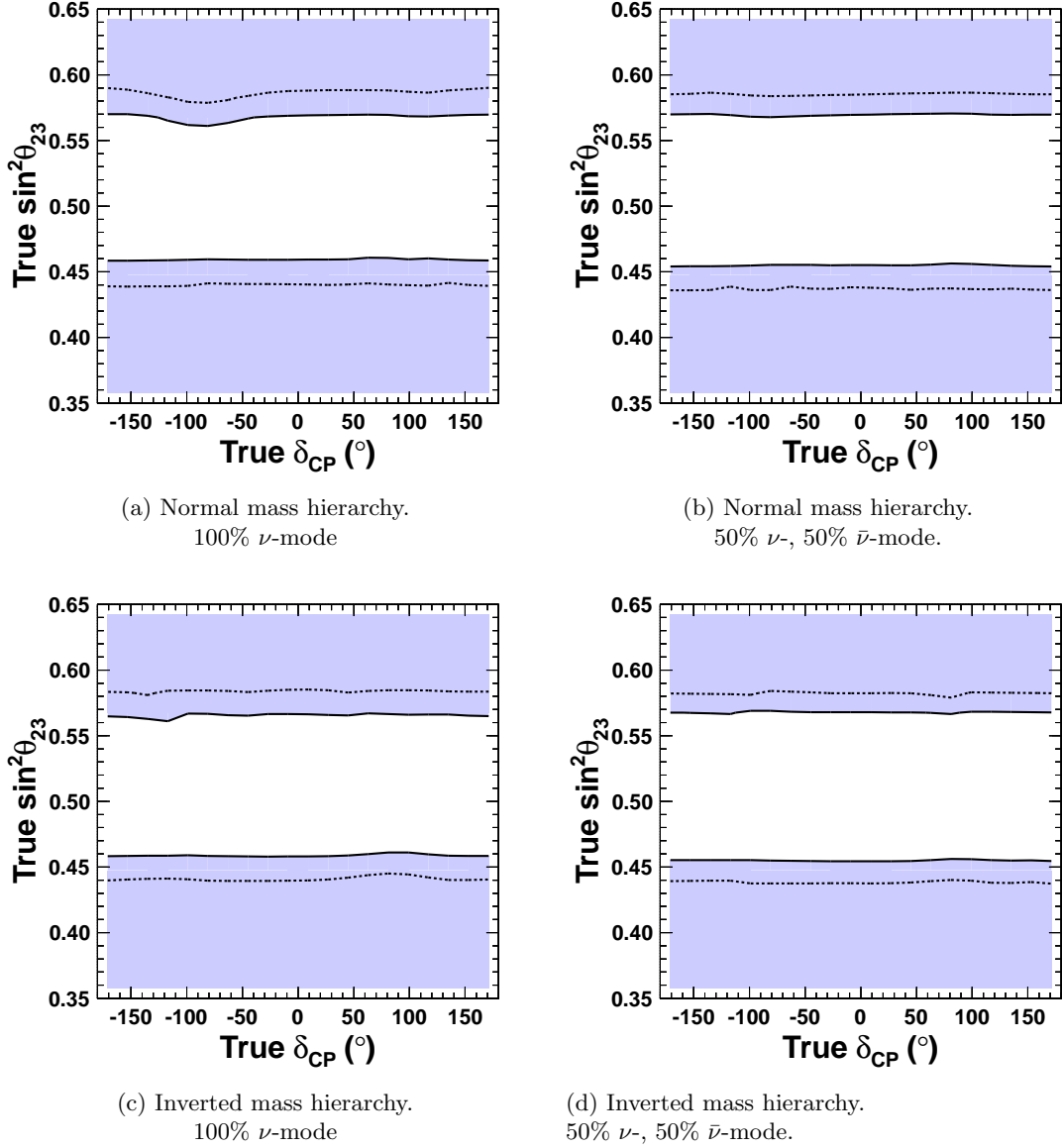


Fig. 10: The region, shown as a shaded area, where T2K has more than a 90 % C.L. sensitivity to reject maximal mixing. The shaded region is calculated assuming no systematic errors (the solid contours show the 90% C.L. sensitivity with statistical error only), and the dashed contours show the sensitivity including the 2012 systematic errors.

335 indicate the earliest case for T2K to observe CP violation. If the systematic error size is  
 336 negligibly small, T2K may reach a higher sensitivity at an earlier stage by running in 100%  
 337  $\nu$ -mode, since higher statistics are expected in this case. However, with projected systematic  
 338 errors, 100%  $\nu$ -mode and 50%  $\nu$ -mode + 50%  $\bar{\nu}$ -mode running give essentially equivalent  
 339 sensitivities.

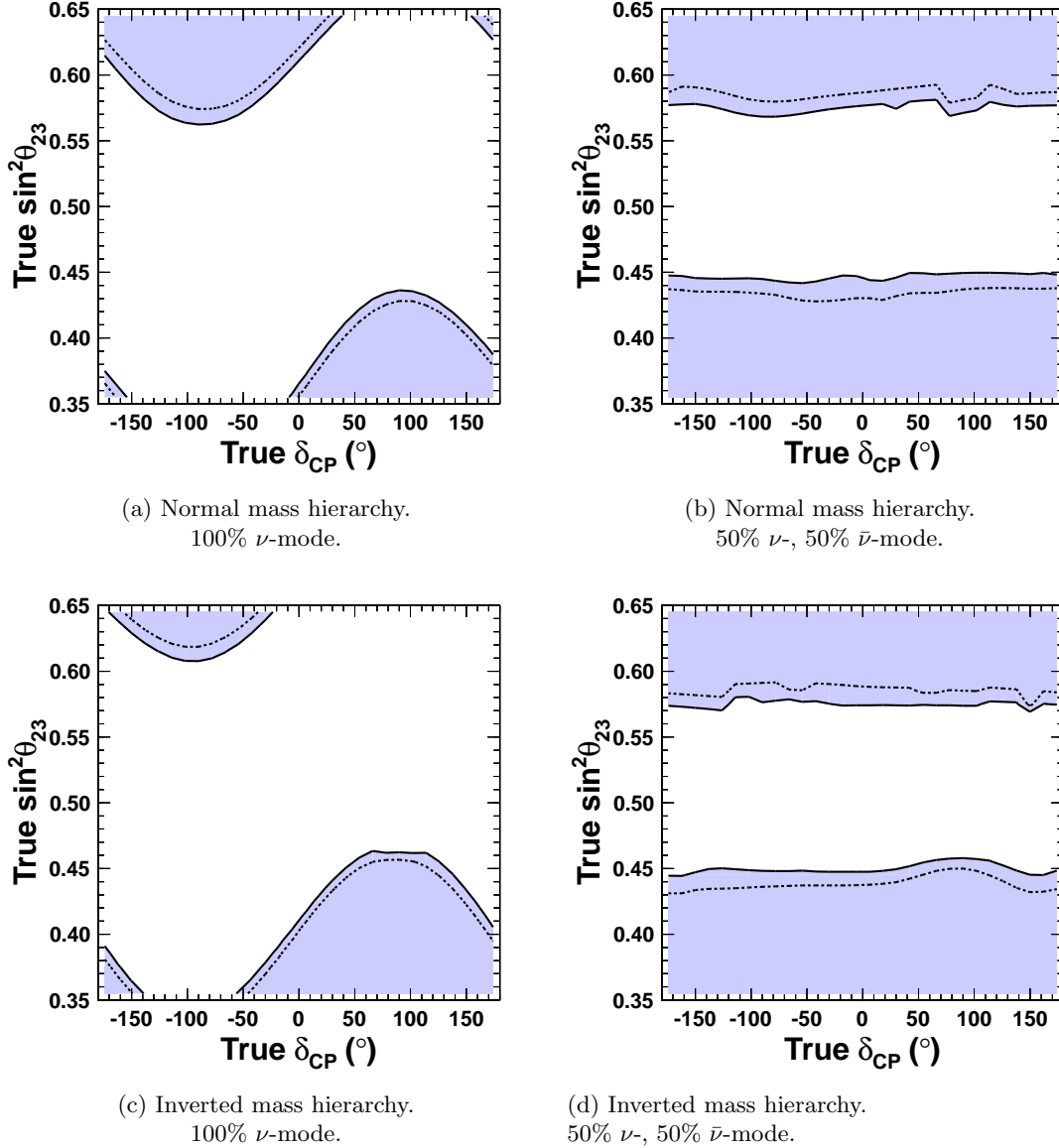


Fig. 11: The region, shown as a shaded area, where T2K has more than a 90% C.L. sensitivity to reject one of the octants of  $\theta_{23}$ . The shaded region is calculated assuming no systematic errors (the solid contours show the 90% C.L. sensitivity with statistical error only), and the dashed contours show the sensitivity including the 2012 T2K systematic errors.

#### 340 4.5. Effect of reduction of the systematic error size

341 An extensive study of the effect of the systematic error size was performed. Although the  
 342 actual effect depends on the details of the errors, here we summarize the results of the  
 343 study. As given in Table 2, the systematic error on the predicted number of events in Super-  
 344 K in the 2012 oscillation analysis is 9.7% for the  $\nu_e$  appearance sample and 13% for the  $\nu_\mu$   
 345 disappearance sample.

346 In Sec. 4.4 we showed the T2K sensitivity with projected systematic errors which are  
 347 estimated based on a conservative expectation of T2K systematic error reduction. In this

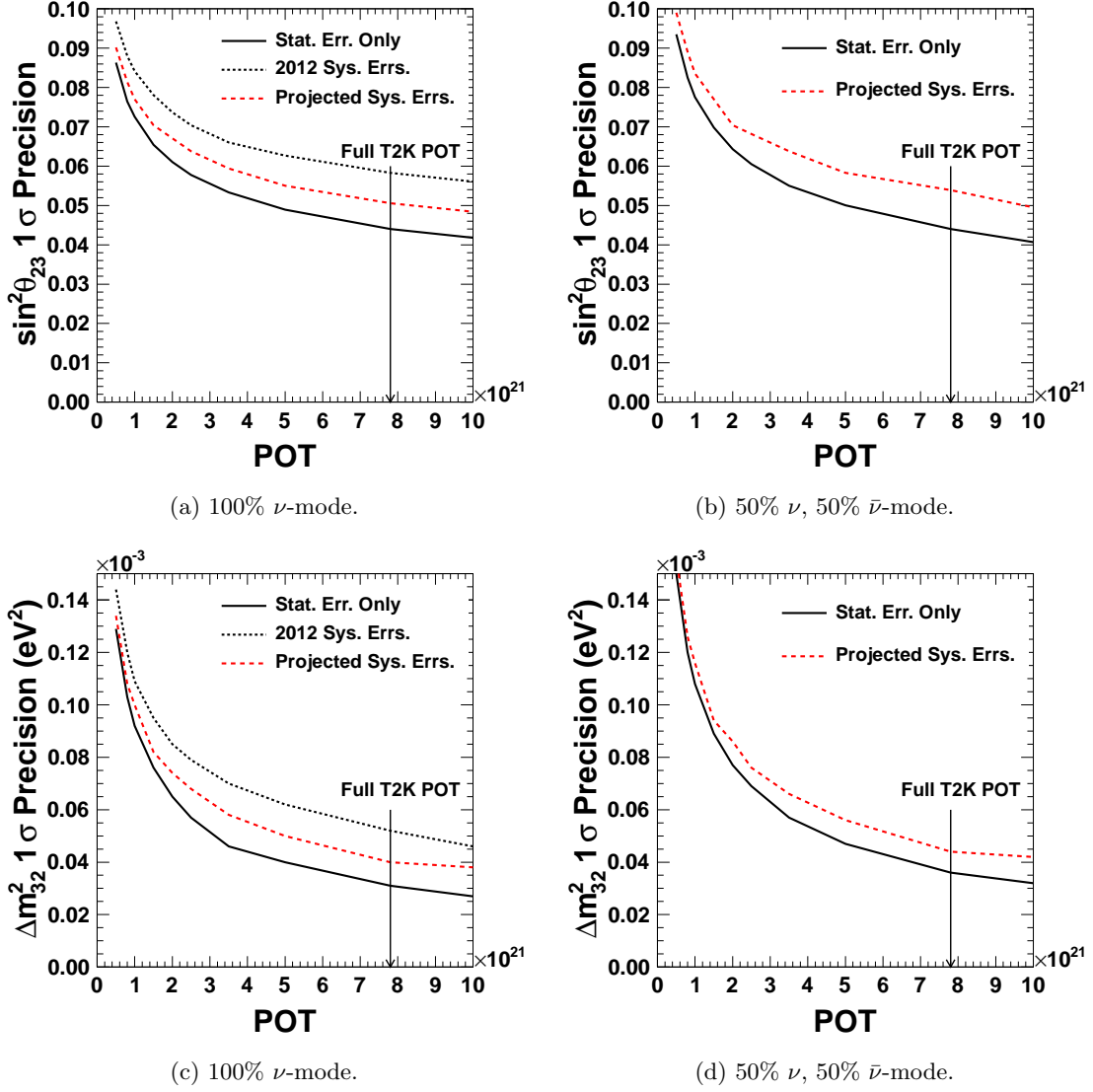


Fig. 12: The uncertainty on  $\sin^2 \theta_{23}$  and  $\Delta m_{32}^2$  plotted as a function of T2K POT. Plots assume the true oscillation parameters given in Table 3. The solid curves include statistical errors only, while the dashed curves assume the 2012 systematic errors (black) or the projected systematic errors (red). A constraint based on the ultimate reactor precision is included.

348 case the systematic error on the predicted number of events in Super-K is about 7% for the  
 349  $\nu_\mu$  and  $\nu_e$  samples and about 14% for the  $\bar{\nu}_\mu$  and  $\bar{\nu}_e$  samples. These errors were calculated  
 350 by reducing the 2012 oscillation analysis errors by removing certain interaction model and  
 351 cross section uncertainties from both the  $\nu_e$ - and  $\nu_\mu$ -mode errors, and by additionally scaling  
 352 all  $\nu_\mu$ -mode errors down by a factor of two. Errors for the  $\bar{\nu}_\mu$ - and  $\bar{\nu}_e$ -modes were estimated  
 353 to be twice those of the  $\nu_\mu$ - and  $\nu_e$ -modes, respectively. These reduced  $\nu$ -mode errors are  
 354 in fact very close to the errors used for the oscillation results reported by T2K in 2014,  
 355 where the T2K oscillation analysis errors have similarly been reduced by improvements in  
 356 understanding the relevant interactions and cross sections.



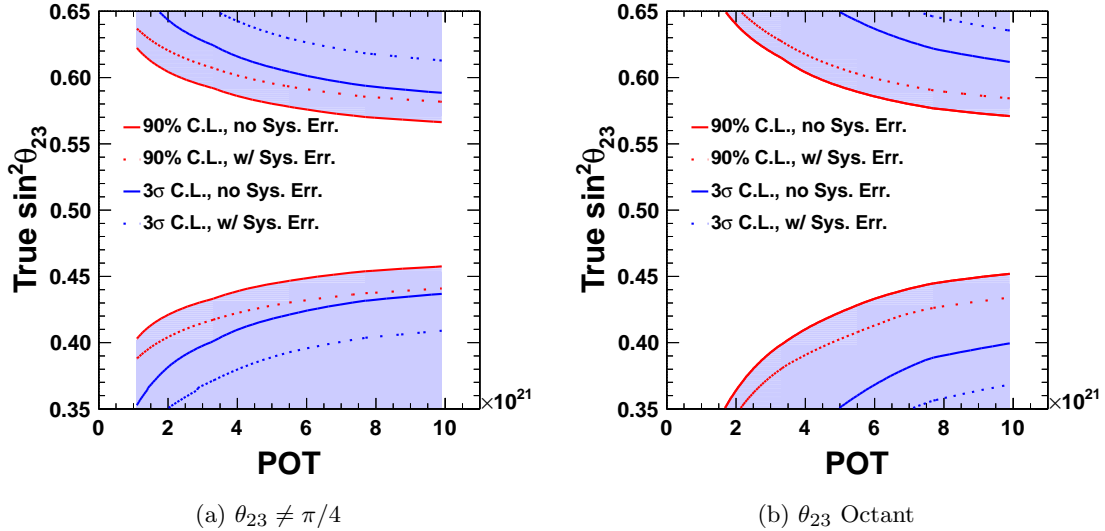


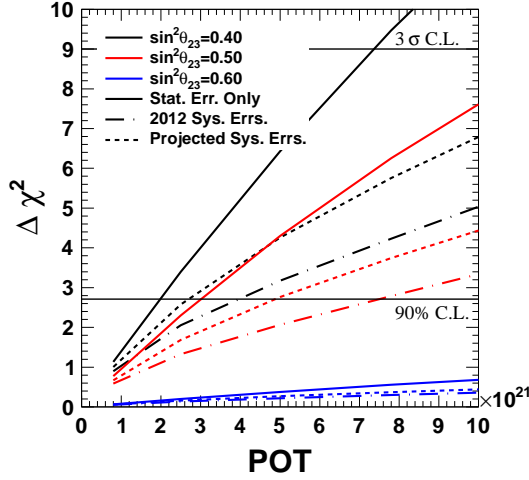
Fig. 13: The region where maximal mixing or one  $\theta_{23}$  octant can be rejected at the stated confidence levels (given by the shaded region), as a function of POT in the case of 50%  $\nu$ -, 50%  $\bar{\nu}$ -mode. These plots are made under the condition that the true mass hierarchy is normal and  $\delta_{CP} = 0$ . The dashed contours include the 2012 systematic errors fully correlated between  $\nu$  and  $\bar{\nu}$ . A constraint based on the ultimate reactor precision is included.

357 For the measurement of  $\delta_{CP}$ , studies have shown that it is desirable to reduce this to  
 358 5~8% for the  $\nu_e$  sample and ~10% for the  $\bar{\nu}_e$  sample to maximize the T2K sensitivity with  
 359 full statistics. The measurement of  $\delta_{CP}$  is nearly independent of the size of the error on  
 360 the  $\nu_\mu$  and  $\bar{\nu}_\mu$  samples as long as we can achieve uncertainty on  $\bar{\nu}_\mu$  similar to the current  
 361 uncertainty on  $\nu_\mu$ . For the measurement of  $\theta_{23}$  and  $\Delta m_{32}^2$ , the systematic error sizes are  
 362 significant compared to the statistical error, and the result would benefit from systematic  
 363 error reduction even for uncertainties as small as 5%.

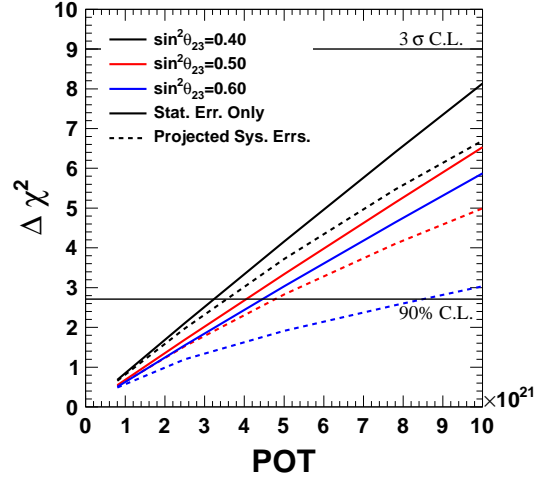
364 These error reductions may also be achievable with the implementation of further T2K  
 365 and external cross section and hadron production measurements, which continue to be made  
 366 with improved precision.

## 367 5. T2K and NO $\nu$ A Combined Sensitivities

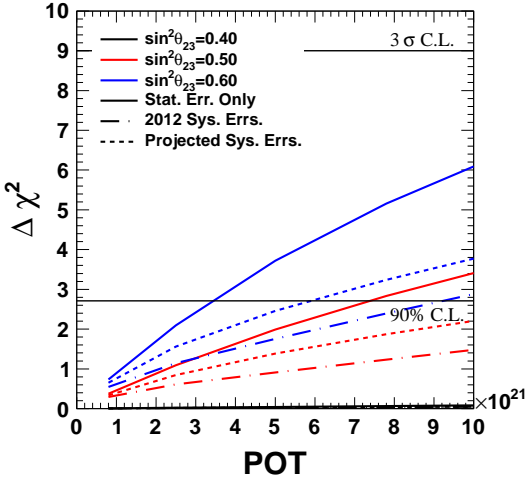
368 The ability of T2K to measure the value of  $\delta_{CP}$  (or determine if CPV exists in the lepton  
 369 sector) is greatly enhanced by the determination of the MH. This enhancement results  
 370 from the nearly degenerate  $\nu_e$  appearance event rate predictions at Super-K in the normal  
 371 hierarchy with positive values of  $\delta_{CP}$  compared to the inverted hierarchy with negative  
 372 values of  $\delta_{CP}$ . Determination of the MH thus breaks the degeneracy, enhancing the  $\delta_{CP}$   
 373 resolution for ~50% of  $\delta_{CP}$  values. T2K does not have sufficient sensitivity to determine the  
 374 mass hierarchy by itself. The NO $\nu$ A experiment [23], which started operating in 2014, has a  
 375 longer baseline (810 km) and higher peak neutrino energy (~ 2 GeV) than T2K. Accordingly,  
 376 the impact of the matter effect on the predicted far detector event spectra is larger in NO $\nu$ A  
 377 (~ 30%) than in T2K (~ 10%), leading to a greater sensitivity to the mass hierarchy. Because  
 378 of the complementary nature of these two experiments, better constraints on the oscillation



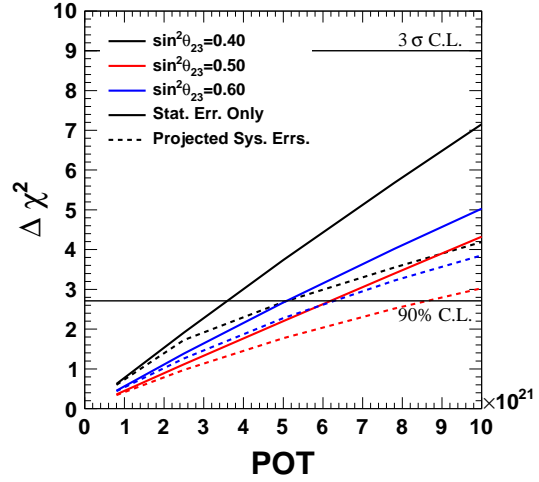
(a) 100%  $\nu$ -mode,  $\delta_{CP} = 90^\circ$ , IH.



(b) 50%  $\nu$ -, 50%  $\bar{\nu}$  running,  $\delta_{CP} = 90^\circ$ , IH.



(c) 100%  $\nu$ -mode,  $\delta_{CP} = -90^\circ$ , NH.



(d) 50%  $\nu$ -, 50%  $\bar{\nu}$  running,  $\delta_{CP} = -90^\circ$ , NH.

Fig. 14: The expected  $\Delta\chi^2$  for the  $\sin\delta_{CP} = 0$  hypothesis, plotted as a function of POT. Plots assume true  $\sin^2 2\theta_{13} = 0.1$ , various true values of  $\sin^2 \theta_{23}$  (as given in the plot legends), and  $\delta_{CP}$  and the MH as given in the figure captions. The solid curves include statistical errors only, while the dash-dotted (dashed) curves assume the 2012 systematic errors (the projected systematic errors). Note that the sensitivity heavily depends on the assumed conditions, and that the conditions applied for these figures correspond to the cases where the sensitivity for  $\sin\delta_{CP} \neq 0$  is maximal.

379 parameters,  $\delta_{CP}$ ,  $\sin^2 \theta_{23}$  and the MH can be obtained by comparing the  $\nu_\mu \rightarrow \nu_e$  oscillation  
 380 probability of the two experiments. To evaluate the benefit of combining the two experiments,  
 381 we have developed a code based on GLOBES [38, 39]. The studies using projected T2K and  
 382 NO $\nu$ A data samples show the full physics reach for the two experiments, individually and  
 383 combined, along with studies aimed at optimization of the  $\nu$ -mode to  $\bar{\nu}$ -mode running ratios  
 384 of the two experiments.

385 Figure 15 shows the relation between the expected number of events of T2K and NO $\nu$ A for  
 386 various values of  $\delta_{CP}$ ,  $\sin^2 \theta_{23}$  and mass hierarchies. The NH and IH predictions occupy dis-  
 387 tinct regions in the plot suggesting how a combined analysis T2K-NO $\nu$ A fit leads to increased  
 388 sensitivity. However, this plot does not include the (statistical + systematic) uncertainties on  
 389 measurements of these event rates. This would result in regions of overlap where the MH can  
 not be determined, and the sensitivity to  $\delta_{CP}$  is degraded. In order to evaluate the effect of

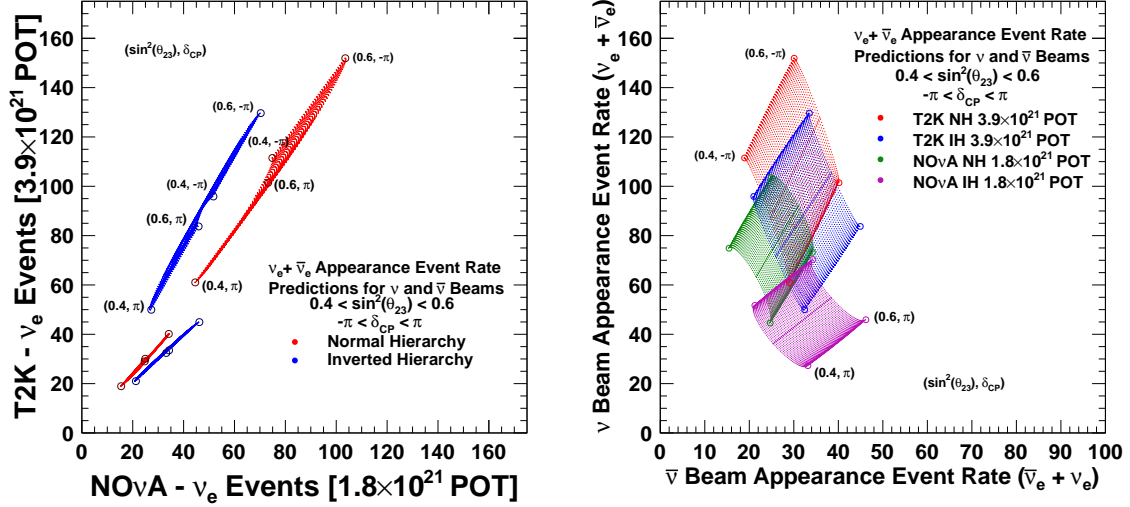


Fig. 15: Relation between the expected number of  $\nu_e + \bar{\nu}_e$  signal events produced by neutrino-mode running and antineutrino mode running in T2K and NO $\nu$ A, for various values of  $\delta_{CP}$ ,  $\sin^2 \theta_{23}$  and mass hierarchy. In the plot of predicted T2K rate versus the predicted NO $\nu$ A rate (left) the blue (IH) and red (NH) upper bands are for neutrino-mode running while the red (NH) and blue (IH) bottom bands are for the antineutrino mode running. The predicted number of  $\nu_e + \bar{\nu}_e$  events produced in neutrino-mode running versus events produced in antineutrino mode running (right) are shown for T2K in red (NH) and blue (IH), and for NO $\nu$ A in green (NH) and magenta (IH). Representative points at the edges of the  $\delta_{CP}$  and  $\sin^2 \theta_{23}$  ranges are highlighted. Systematic and statistical uncertainties are not included.

390 combining the results from T2K and NO $\nu$ A quantitatively, we have conducted a T2K-NO $\nu$ A  
 391 combined sensitivity study. The GLOBES [38, 39] software package was used to fit oscillation  
 392 parameters based on the reconstructed neutrino energy spectra of the two experiments. The  
 393 fits were conducted by minimizing  $\Delta\chi^2$  which is calculated from spectra generated with dif-  
 394 ferent sets of oscillation parameters, and includes penalty terms for deviations of the signal  
 395 and background normalizations from nominal. The best-fit  $\Delta\chi^2$  calculated by GLOBES, was  
 396 the metric chosen to characterize sensitivity, as it is related to the probability that a given  
 397 data set can result from two different hypotheses.  
 398

399 GLOBES combines flux, cross section, energy resolution/bias and efficiency information  
 400 for an experiment to estimate energy spectra of neutrino interaction samples used for anal-  
 401 yses. Then GLOBES uses a full three-flavor oscillation probability formulation to fit analysis  
 402 spectra generated assuming different oscillation parameters to each other (varying oscillation

parameter values and parameters accounting for systematic uncertainties within their uncertainties). The oscillation parameters, unless otherwise stated, are those shown in Table 3. The GLoBES three-flavor analysis package works very similarly to fitter used for the studies presented in Section 4. Several validation studies were done to ensure that the two methods produced the same results when given the same inputs.

The T2K, NO $\nu$ A, and combined sensitivities were generated using a modified version of GLoBES that allowed for use of inputs generated from Monte Carlo simulations of T2K neutrino interactions in the Super-Kamiokande detector. The inputs describing the NO $\nu$ A experiment were developed in conjunction with NO $\nu$ A collaborators, and validated against official NO $\nu$ A sensitivity plots [40, 41, 42]. We assume the same run plan as presented in NO $\nu$ A’s TDR:  $1.8 \times 10^{21}$  POT for  $\nu$  and  $1.8 \times 10^{21}$  POT for  $\bar{\nu}$  modes, corresponding to 3 years of running in each mode.

The GLoBES inputs defining the analysis sample acceptances for the signal, the NC background, the  $\nu_\mu$  CC background, and the  $\nu_e$  CC background were tuned to match this official event rate prediction from NO $\nu$ A. For example, Table 6 summarizes the expected number of  $\nu_e$  appearance events for NO $\nu$ A [42] when  $\sin^2 2\theta_{13} = 0.95$  is assumed and the solar oscillation terms or matter effects in the oscillation probability are neglected.

Table 6: Expected number of  $\nu_e$  appearance signal and background events for NO $\nu$ A at  $1.8 \times 10^{21}$  POT for each of  $\nu$  and  $\bar{\nu}$  modes[42]. The oscillation probabilities used to calculate the predicted number of events assumed  $\sin^2 2\theta_{13} = 0.095$  and do not include the solar oscillation terms or matter effects.

Beam	Signal	NC Bkg	$\nu_\mu$ CC	$\nu_e$ CC	Total Bkg
$\nu$ -mode	72.6	20.8	5.2	8.4	34.5
$\bar{\nu}$ -mode	33.8	10.6	0.7	5.0	16.3

Since NO $\nu$ A has only recently began taking data, detailed evaluation of systematic uncertainties is not yet published. Therefore, the combined sensitivity studies used a simplified systematics treatment for both T2K and NO $\nu$ A: a 5% normalization uncertainty on signal events and a 10% normalization uncertainty on background events for both appearance and disappearance spectra. Uncertainties that impact the spectral shape are not considered. This is a reasonable choice since both experiments use a narrow band beam and much of the oscillation sensitivity comes from the measured event rates. The uncertainties are assumed to be uncorrelated for  $\nu_e$  appearance,  $\bar{\nu}_e$  appearance,  $\nu_\mu$  disappearance, and  $\bar{\nu}_\mu$  disappearance. This simple systematics implementation, referred to in the rest of the paper as “normalization systematics”, is the same as the one adopted in the NO $\nu$ A TDR and is also a reasonable representation of the projected uncertainties at T2K. The sensitivities shown here are obtained assuming  $\sin^2 2\theta_{13} = 0.1$  with the projected reactor constraint of 5%.

When determining the MH,  $\Delta\chi^2$  is not distributed according to a  $\chi^2$  distribution because the MH is a discrete, rather than a continuous, variable. Toy MC studies, where many pseudo-experiments are generated with statistical and systematic fluctuations, were used to evaluate the validity of applying a  $\Delta\chi^2$  test statistic, as given in Eq. 5, for the MH determination.

Table 7: Values of  $T_{MC}$  and  $T_{Median}$  and their associated p-values. The  $T$  values correspond to the vertical lines shown in Fig.16. The p-values are computed either with a  $\chi^2$  distribution for one degree of freedom from the spectra at the toy MC statistical mean or using an ensemble of toy MC experiments.

	by MC mean spectra		by toy MC experiments	
	$T_{MC}$	p-value( $\chi^2$ )	$T_{Median}$	p-value(toy MC)
NH, $\delta_{CP} = -90^\circ$	11.4	0.00073	11.8	0.000065
NH, $\delta_{CP} = 0^\circ$	3.22	0.073	3.57	0.019
NH, $\delta_{CP} = +90^\circ$	3.47	0.063	2.34	0.040
IH, $\delta_{CP} = -90^\circ$	3.33	0.068	2.30	0.042
IH, $\delta_{CP} = 0^\circ$	3.19	0.074	3.79	0.015
IH, $\delta_{CP} = +90^\circ$	11.6	0.00067	12.5	0.000031

437 The left column of Fig. 16 shows distributions for a test static for  $H_0 = \text{IH}$ :

$$T = \chi_{IH}^2 - \chi_{NH}^2, \quad (6)$$

438 where  $\chi_{IH}^2$  and  $\chi_{NH}^2$  are the minimum  $\chi^2$  values obtained by fitting the oscillation parameters  
439 while fixing the MH to the inverted or normal mass hierarchy, respectively. This  $T$  is plotted  
440 here instead of  $\Delta\chi^2$  for easier interpretation. In the figure, the blue (red) distributions are  
441 for the case where test or ‘observed’ spectra were generated for the inverted (normal) mass  
442 hierarchy with statistical and systematic fluctuations. Except for  $\delta_{CP}$ , the test oscillation  
443 parameters were fixed to the nominal values given in Table 3. The value of  $\delta_{CP}$  was fixed to  
444 that given in each caption for the NH, while it was thrown over all values of  $\delta_{CP}$  for the IH.  
445 This is done in order to calculate the p-value for  $H_0 = \text{IH}$  with unknown  $\delta_{CP}$  when the test  
446 point is in the NH [43]. The right column of Figure 16 is the same, but with the opposite  
447 MH hypothesis test ( $H_0 = \text{NH}$ ):

$$T = \chi_{NH}^2 - \chi_{IH}^2 \quad (7)$$

448 with a test point in the IH. The  $T$ -value calculated using the spectrum generated from  
449 the MC sample statistical mean ( $T_{MC}$ ), which is generally used in this paper, is compared  
450 with the median  $T$ -value for the ensemble of toy MC experiments ( $T_{median}$ ) in Table 7 for  
451 different oscillation parameter sets. The p-values calculated for  $T_{MC}$ , assuming that  $\Delta\chi^2$   
452 follows a true  $\chi^2$  distribution, compared with the p-values calculated as the fraction of the  
453  $T$  distribution for  $H_0 = (\text{correct MH})$  above  $T_{median}$  are also given.

454 Figures 17 through 19 show plots of expected C.L. contours for T2K, NO $\nu$ A and a T2K-  
455 NO $\nu$ A combined fits as functions of  $\sin^2\theta_{23}$  vs.  $\delta_{CP}$ . Regions where  $\sin\delta_{CP} = 0$ , one MH  
456 and one  $\theta_{23}$  octant are expected to be ruled out at the 90% C.L are shown. Significantly  
457 wider regions are covered by combining the results from T2K and NO $\nu$ A.

458 In Figures 20 and 21 the  $\Delta\chi^2$  for  $\sin\delta_{CP} = 0$  and for each MH is plotted as a function  
459 of ‘true’  $\delta_{CP}$  in case of  $\sin^2(\theta_{23}) = 0.5$ . The ‘true’ value of  $\sin^2(\theta_{23}) = 0.5$  was chosen to  
460 present a simplified view of the sensitivities for maximal mixing. The T2K’s  $\Delta\chi^2$  is smaller at  
461  $\delta_{CP} = +90^\circ(-90^\circ)$  compared to that at the opposite sign of  $\delta_{CP} = -90^\circ(+90^\circ)$  for NH(IH)  
462 case while those are similar for NO $\nu$ A. This comes from the large degeneracy between the  
463 CP-violating term and the matter effect for T2K. In case of NO $\nu$ A, the matter effect is large

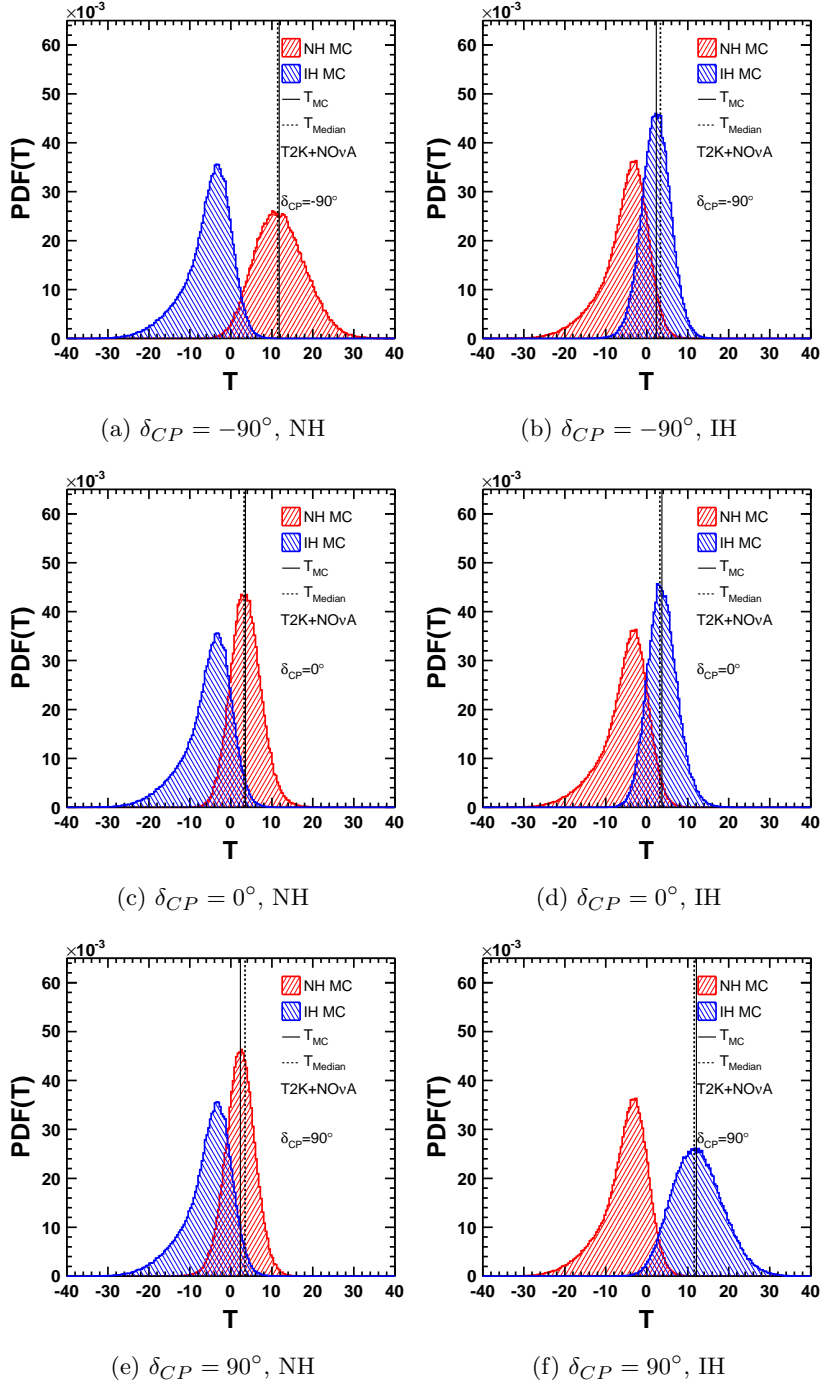


Fig. 16: Distributions of the test statistic,  $T$  for toy MC experiments with the null hypothesis  $H_0 = \text{I(N)H}$  are shown in the left (right) column. Toy MC experiments are generated with the nominal oscillation parameters except for the MH and  $\delta_{CP}$ ; those generated with NH are indicated in red and those with IH in blue. The value of  $\delta_{CP}$  is fixed to the value indicated in the sub-captions when  $H_0 =$  (correct MH), but thrown when  $H_0 =$  (incorrect MH), where the correct MH is also given in the sub-captions. Solid lines indicate the value of the MH determination sensitivity metric used in this paper (calculated using the spectra at the MC sample statistical mean), and dashed lines indicate the  $T$ -value for the median of the toy MC distribution.

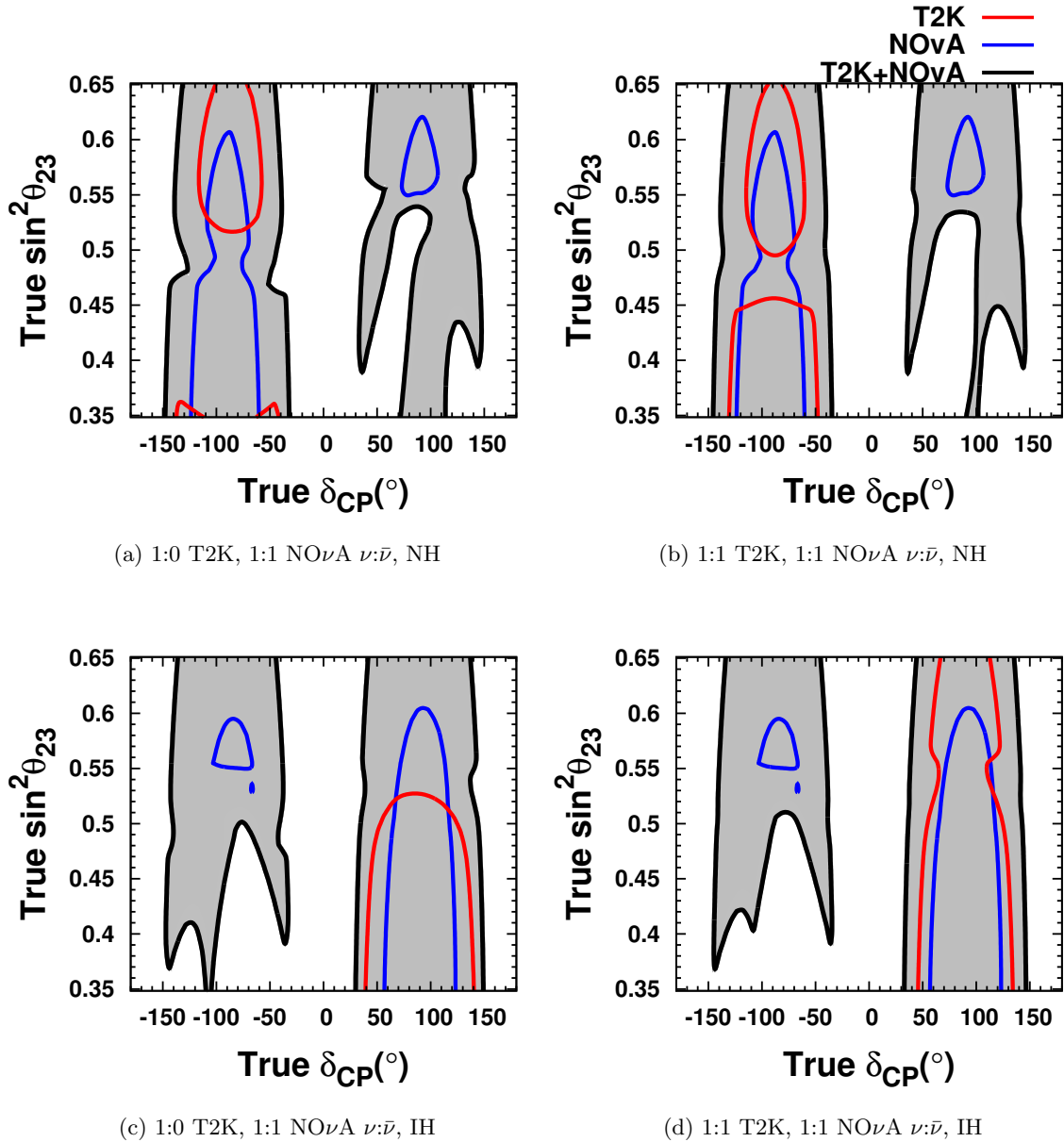


Fig. 17: Regions where T2K (red), NOνA (blue), and T2K+NOνA (black) is predicted to rule out  $\sin \delta_{CP} = 0$  at 90% C.L. Points within the gray regions are where  $\sin \delta_{CP} = 0$  is predicted to be rejected at 90% C.L. for T2K+NOνA, assuming simple normalization systematics as described in the text.

464 enough that the degenerate parameters space is much smaller as can be seen in Fig. 15. The  
 465 complex structure for positive (negative) values of  $\delta_{CP}$  with a true NH (IH) is also due to  
 466 the fact that  $\Delta\chi^2$  calculation profiles over MH, and the expected number of  $\nu_e$  appearance  
 467 events is nearly degenerate in these regions. T2K would perform better than or comparable  
 468 to NOνA, if the MH was assumed to be known. However, there is no experiment, besides  
 469 NOνA, that expects to determine the MH on the relevant time scale, thus the case of a known  
 470 MH is not presented. These figures demonstrate the sensitivity of the two experiments, as

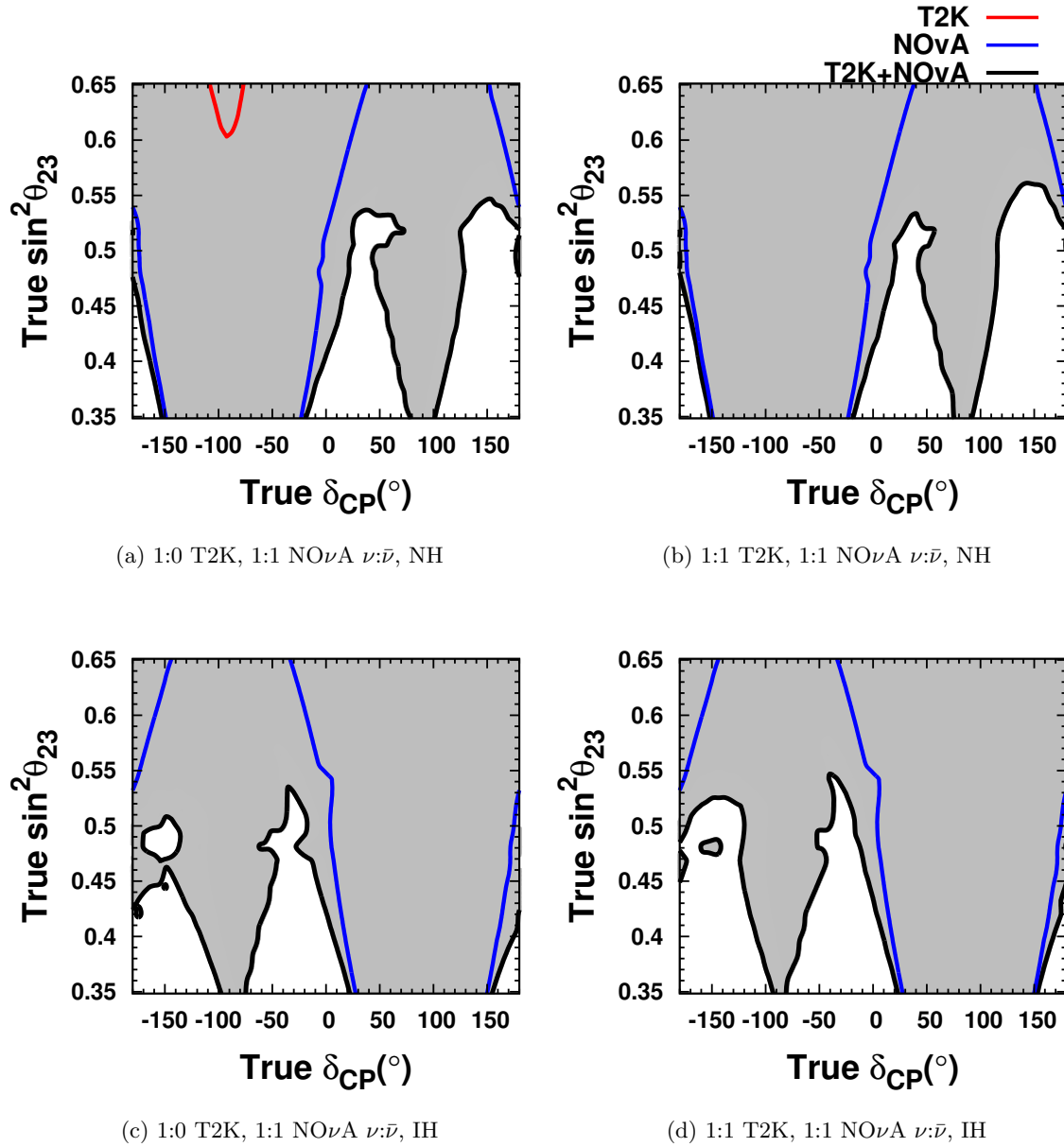


Fig. 18: Regions for T2K (red), NOνA (blue), and T2K+NOνA (black) where the incorrect Mass Hierarchy is predicted to be rejected at 90% C.L. Points within the gray regions are where the incorrect mass hierarchy is predicted to be rejected at 90% C.L. for T2K+NOνA, assuming simple normalization systematics as described in the text.

471 well as the benefit of combined analysis of the two data sets on the ability to determine MH  
 472 and CPV.

## 473 6. Neutrino Mode and Antineutrino Mode Running Time Optimization

474 As previously shown in Sec. 4, a significant fraction of  $\bar{\nu}$ -mode running improves the sensi-  
 475 tivity to CP violation, especially when systematic uncertainties are taken into account. In  
 476 this section studies of the  $\nu:\bar{\nu}$  running ratios are shown for T2K, NOνA, and combined fits of



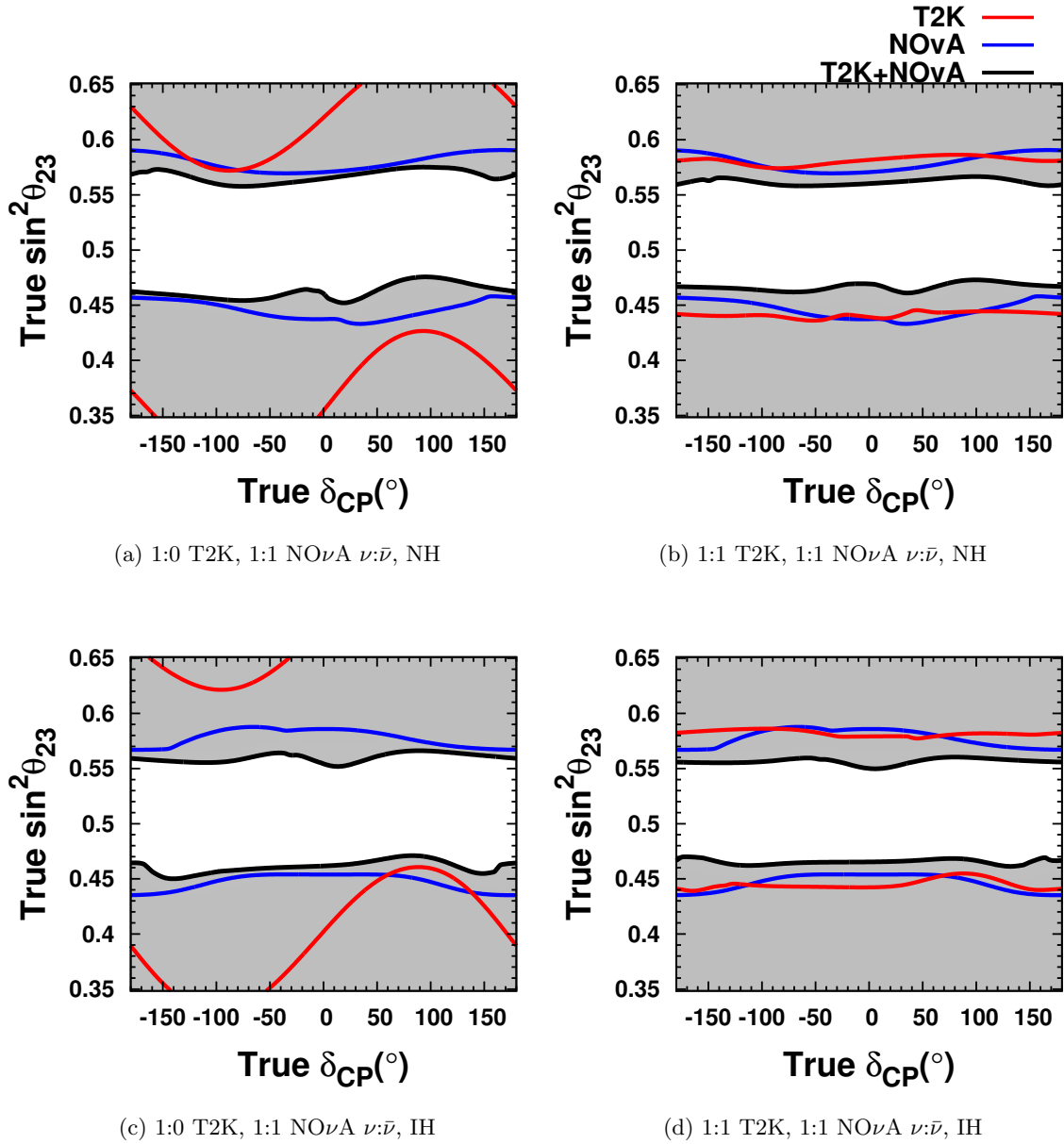


Fig. 19: Regions for T2K (red), NO $\nu$ A (blue), and T2K+NO $\nu$ A (black) where the incorrect octant is predicted to be rejected at 90% C.L. Points inside the gray regions are where the incorrect octant is predicted to be rejected at 90% C.L. for T2K+NO $\nu$ A assuming simple normalization systematics as described in the text.

477 T2K+NO $\nu$ A simulated data using the tools developed in Sec. 5. A set of metrics are defined  
 478 that characterize the ability of each experiment or a combined fit of both experiments to  
 479 constrain  $\delta_{CP}$ , reject  $\delta_{CP} = 0$ , or determine the MH. The following metrics are used in these  
 480 studies:

- 481  $\circ$   $\delta_{CP}$  half-width: The  $1\sigma$  half-width is defined as half of the  $1\sigma$  Confidence Interval (C.I.)  
 482 about the true value of  $\delta_{CP}$ . In some cases there are degenerate  $1\sigma$  C.I. regions in  
 483  $\delta_{CP}$  that are disconnected from the central value. In this case half of the width of the

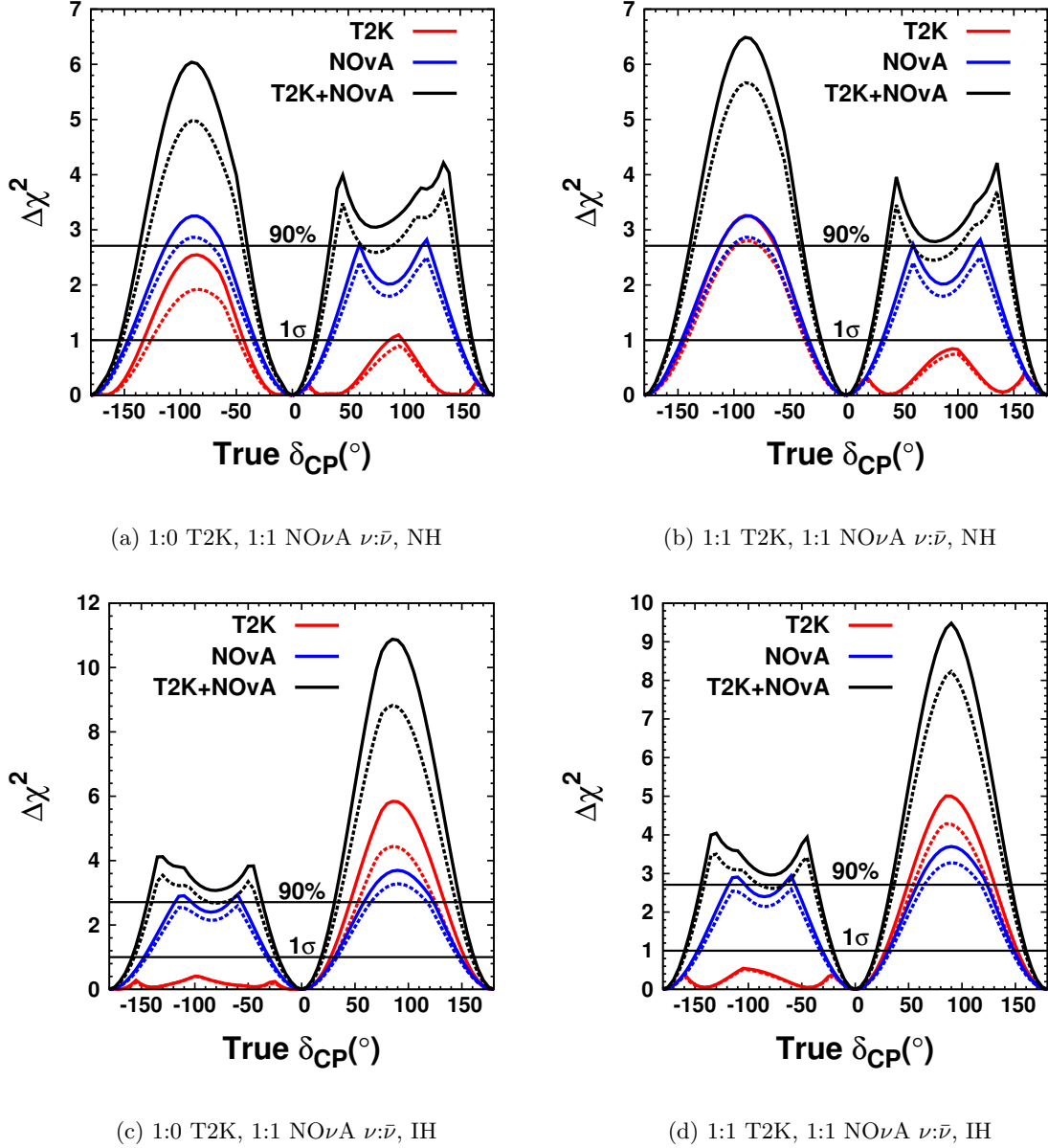


Fig. 20: The predicted  $\Delta\chi^2$  for rejecting  $\sin\delta_{CP} = 0$  hypothesis, as a function of  $\delta_{CP}$  for T2K (red), NOνA (blue), and T2K+NOνA (black). Dashed (solid) curves indicate studies where normalization systematics are (not) considered. The ‘true’ value of  $\sin^2(\theta_{23})$  is assumed to be 0.5, and the ‘true’ MH is assumed to be the NH (top) or the IH (bottom). The ‘test’ MH is unconstrained.

- 484 degenerate region is added to this metric. This is a measure of the precision that can be  
 485 achieved in measurement of  $\delta_{CP}$ .
- 486 ○ Median  $\Delta\chi^2$  for  $\delta_{CP} = 0$ : This metric defines the  $\Delta\chi^2$  value for which 50% of true  $\delta_{CP}$   
 487 values can be distinguished from  $\delta_{CP} = [0, \pi]$ . This is a measure of sensitivity to CPV.
  - 488 ○ Lowest  $\Delta\chi^2$  for mass hierarchy determination: This metric defines the  $\Delta\chi^2$  value at  
 489 which the mass hierarchies can be distinguished for 100% of true  $\delta_{CP}$  values.

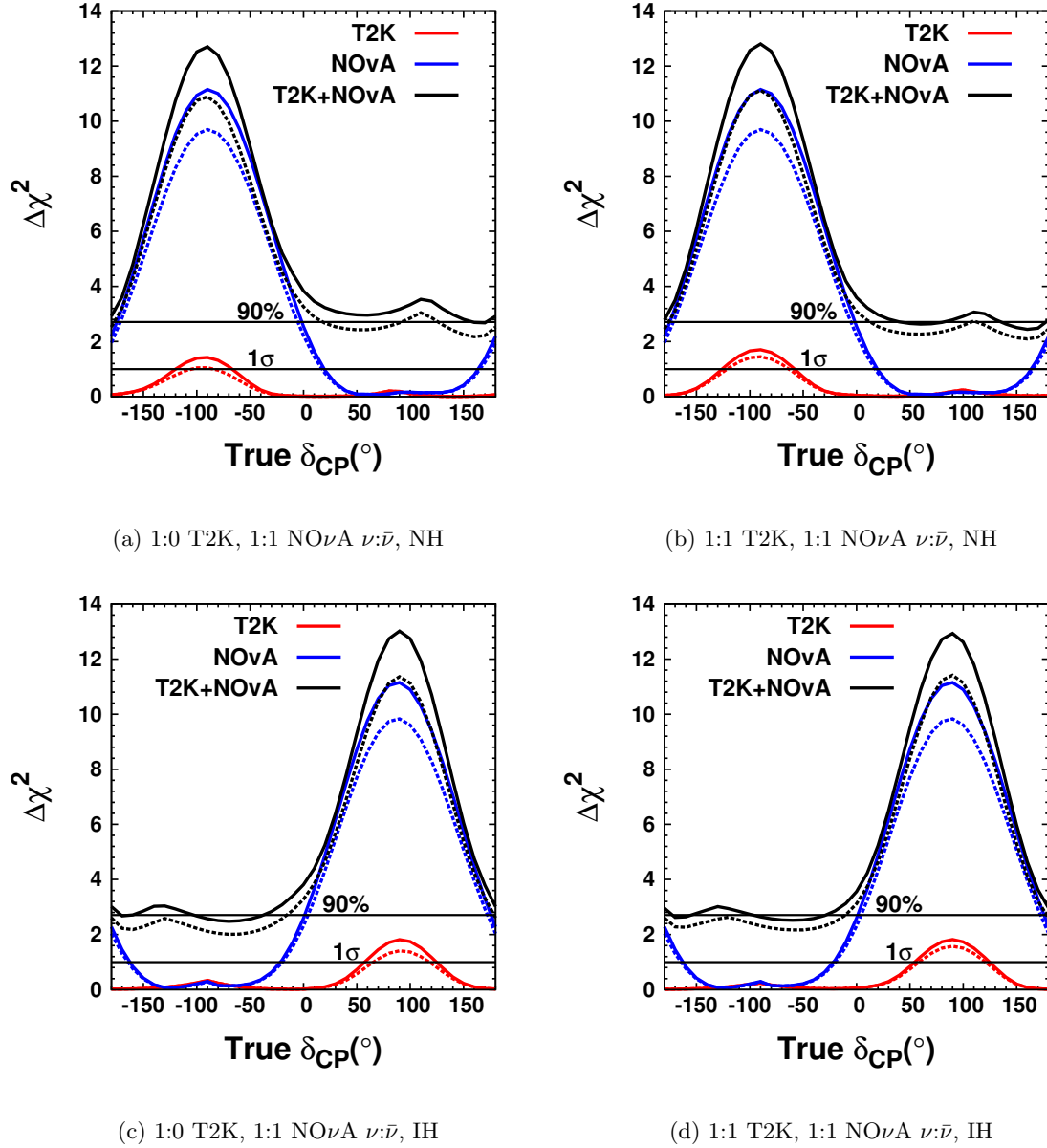


Fig. 21: The predicted  $\Delta\chi^2$  for rejecting the incorrect MH hypothesis, as a function of  $\delta_{CP}$  for T2K (red), NOνA (blue), and T2K+NOνA (black). Dashed (solid) curves indicate studies where normalization systematics are (not) considered. The ‘true’ value of  $\sin^2(\theta_{23})$  is assumed to be 0.5, and the ‘true’ MH is assumed to be the NH (top) or the IH (bottom). The ‘test’ MH is unconstrained.

490 Each metric is calculated for a T2K+NOνA combined analysis for various  $\nu:\bar{\nu}$  run ratios.  
 491 Figure 22 gives the lowest  $\Delta\chi^2$  values for mass hierarchy determination for  $\nu:\bar{\nu}$  variations  
 492 in a combined T2K+NOνA fit. They are computed from the results of studies like the  
 493 one shown in Fig. 21 and conservatively summarize the content of the plot in one data  
 494 point. For example, the lowest  $\Delta\chi^2$  value for mass hierarchy determination at 1:0 (100%  $\nu$

495 running) T2K, 5:5 (50%  $\nu$  / 50%  $\bar{\nu}$  running) NO $\nu$ A running is the lowest  $\Delta\chi^2$  from Fig. 21(a)  
 ( $\Delta\chi^2 = 2.19$ ).

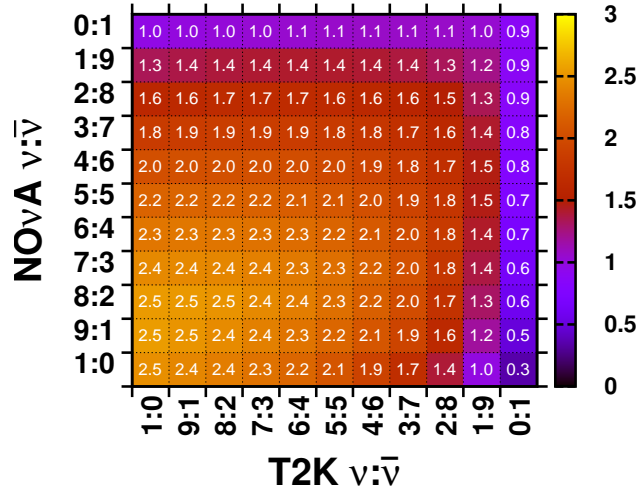


Fig. 22: Lowest  $\Delta\chi^2$  for a combined T2K+NO $\nu$ A fit to determine the mass hierarchy for various  $\nu:\bar{\nu}$  running ratios. True values are assumed to be: MH=NH,  $\sin^2(\theta_{23}) = 0.5$ . Normalization systematics are assumed.

496 Similarly, Fig. 23 gives the median  $\Delta\chi^2$  values for  $\sin\delta_{CP} = 0$  for  $\nu:\bar{\nu}$  variations in a  
 497 combined T2K+NO $\nu$ A fit. These values are computed from studies like the ones presented  
 498 in Fig. 20. The  $\sin\delta_{CP} = 0$  median  $\Delta\chi^2$  value at 1:0 T2K, 5:5 NO $\nu$ A running is the median  
 499  $\Delta\chi^2$  from Fig. 20(a) ( $\Delta\chi^2 = 2.6$ ).  
 500

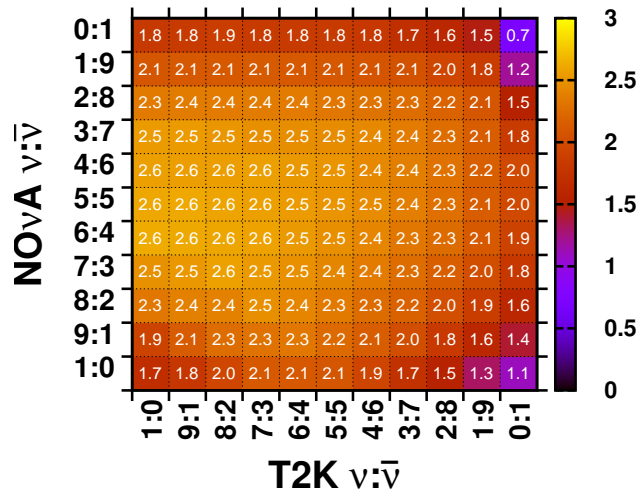


Fig. 23: Median  $\Delta\chi^2$  for  $\sin\delta_{CP} = 0$  for a combined T2K+NO $\nu$ A fit. True values are assumed to be: MH=NH,  $\sin^2(\theta_{23}) = 0.5$ . Normalization systematics are assumed.

501 Figure 24 summarizes the data in Fig. 22 and compares it with the metric calculated  
 502 for T2K only running. The black curve gives the lowest  $\Delta\chi^2$  for MH determination in a  
 503 combined, T2K+NO $\nu$ A, fit as a function of T2K  $\nu:\bar{\nu}$  running ratio with the NO $\nu$ A running  
 504 fixed at 1:1. As shown previously, the T2K data set alone has almost no sensitivity to the  
 505 MH determination. The curves for 5:5 NO $\nu$ A running with systematics (black dashed) shows  
 506 an optimal T2K running ratio of around 6:4 for a combined fit. However, the metric is very  
 507 flat with respect to the T2K  $\nu:\bar{\nu}$  run ratio for  $\nu$  running greater than 50%. Figure 25 shows  
 508 the summary for median  $\Delta\chi^2$  for  $\sin\delta_{CP} = 0$ . T2K run ratios between 1:0 and 5:5 produce  
 509 relatively similar values of median  $\Delta\chi^2$  for the combined fit. This is also true for combined  
 510 T2K+NO $\nu$ A running independent of the NO $\nu$ A run plan optimization. There is a slight  
 511 preference for all neutrino running in T2K in the combined fit.

512 Figure 26 and 27 summarize the  $\delta_{CP}$   $1\sigma$  width at various values of  $\delta_{CP}$ . Again, relatively  
 513 similar values of  $\delta_{CP}$   $1\sigma$  width are expected for the T2K run ratios between 1:0 and 1:9.

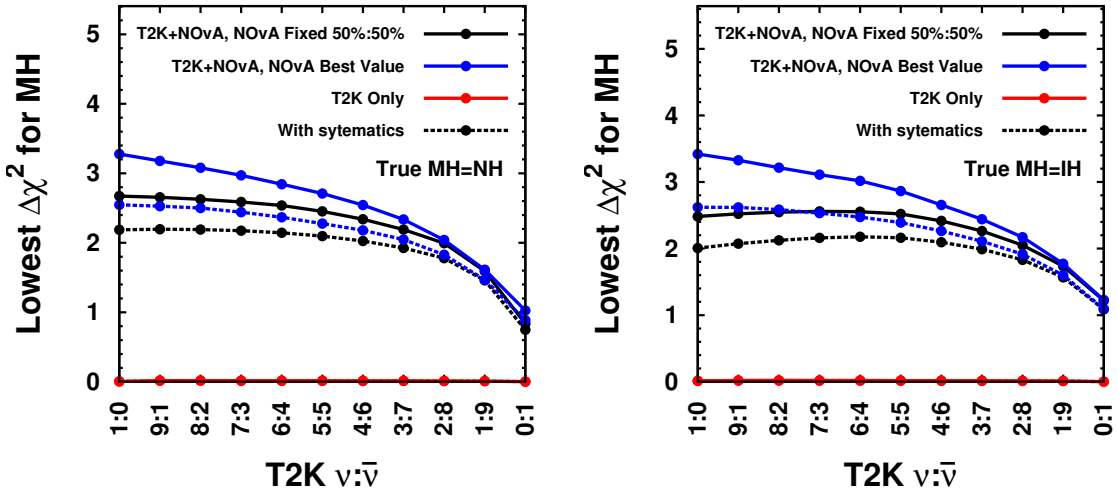


Fig. 24: Lowest  $\Delta\chi^2$  for mass hierarchy determination in a combined, T2K+NO $\nu$ A, fit as a function of T2K  $\nu:\bar{\nu}$  running ratio for true MH=NH (left) and IH (right). Curves are given for the  $\Delta\chi^2$  value at nominal 5:5 NO $\nu$ A running (black), best case T2K+NO $\nu$ A running (blue), and T2K only running (red). Dashed (solid) curves indicate studies performed (without) assuming normalization systematics.

514 All of the metrics demonstrate a relatively flat response between approximately 7:3 and  
 515 3:7 for T2K and for T2K+NO $\nu$ A (5:5) with systematics, with a worse response outside that  
 516 range. These results are consistent with several other studies not shown in this paper (e.g.  
 517 the measures of the precision on  $\sin^2\theta_{13}$  in  $\nu$ -mode and in  $\bar{\nu}$ -mode). The results are also  
 518 robust with respect to reasonable variations in  $\sin^2\theta_{23}$ ,  $\delta_{CP}$  and the MH. Thus, the results  
 519 suggest that T2K run with a  $\nu$ -mode to  $\bar{\nu}$ -mode at ratio of 1:1 with an allowed variation  
 520 of  $\pm 20\%$  of the total exposure. The variation can be used to optimize the experiment to  
 521 any one analysis without significant degradation of the sensitivity to any other analysis. A  
 522 more detailed optimization of the  $\nu:\bar{\nu}$  run ratio will require tighter constraints on oscillation

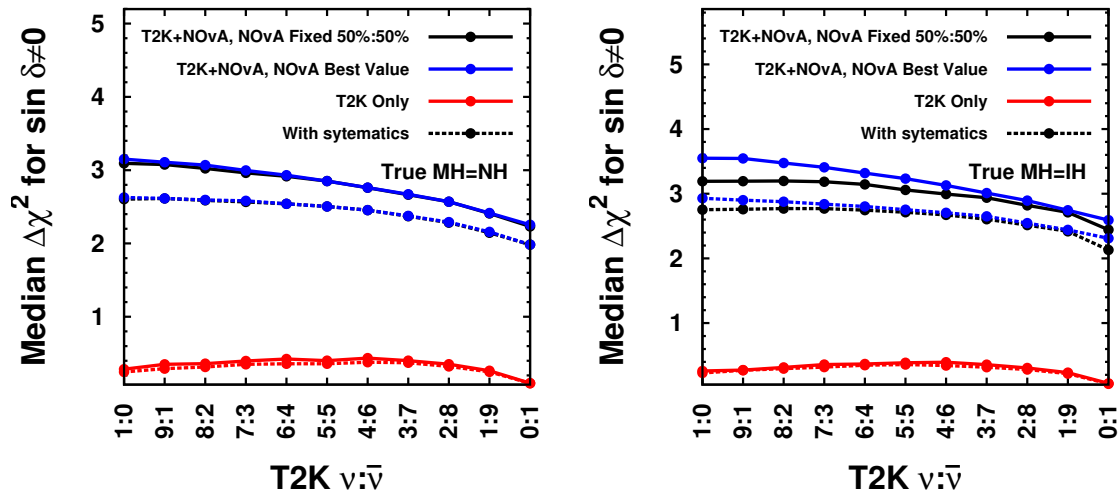


Fig. 25: Median  $\Delta\chi^2$  for  $\sin\delta_{CP} = 0$  in a combined, T2K+NO $\nu$ A, fit as a function of T2K  $\nu:\bar{\nu}$  running ratio for true MH=NH (left) and IH (right). Curves are given for the  $\Delta\chi^2$  value at nominal 5:5 NO $\nu$ A running (black), best case T2K+NO $\nu$ A running (blue), and T2K only running (red). Dashed (solid) curves indicate studies performed (without) assuming normalization systematics.

523 parameters from future analyses, a more detailed treatment of systematic uncertainties from  
 524 both T2K and NO $\nu$ A, and a clear prioritization of analysis goals from the T2K and NO $\nu$ A  
 525 collaborations.

## 526 7. Summary

527 In this paper we have presented studies of the T2K experiment sensitivity to oscillation  
 528 parameters by performing a three-flavor analysis combining appearance and disappearance,  
 529 for both  $\nu$ -mode, and  $\bar{\nu}$ -mode assuming the expected full statistics of  $7.8 \times 10^{21}$  POT. The  
 530 T2K precision study includes either statistical errors only, systematic errors established  
 531 for the 2012 oscillation analyses, or conservatively projected systematic errors, and takes  
 532 into consideration signal efficiency and background. We have derived the sensitivity to the  
 533 oscillation parameters  $\sin^2 2\theta_{13}$ ,  $\delta_{CP}$ ,  $\sin^2 2\theta_{23}$ , and  $\Delta m_{32}^2$  for a range of the true parameter  
 534 values and using constraints from other experiments. For example, with equal exposure of  
 535  $\nu$ -mode and  $\bar{\nu}$ -mode and using signal efficiency from the 2012 analysis we project a dataset  
 536 of approximately 100  $\nu_e$  and 25  $\bar{\nu}_e$  appearance events and 390 (270)  $\nu_\mu$  and 130 (70)  $\bar{\nu}_\mu$   
 537 CCQE (CC non-QE) events. From these data, with the projected systematic uncertainties  
 538 we would achieve a 1- $\sigma$  resolution of 0.050(0.054) on  $\sin^2 \theta_{23}$  and  $0.040(0.045) \times 10^{-3} \text{eV}^2$   
 539 on  $\Delta m_{32}^2$  for 100%(50%) neutrino beam mode running. T2K will also have sensitivity to  
 540 the CP-violating phase  $\delta_{CP}$  at 90% C.L. or higher over a significant range. For example, if  
 541  $\sin^2 \theta_{23}$  is maximal (i.e.  $\theta_{23}=45^\circ$ ) the range is  $-115^\circ < \delta_{CP} < -60^\circ$  for normal hierarchy and  
 542  $+50^\circ < \delta_{CP} < +130^\circ$  for inverted hierarchy.

543 Since the ability of T2K to measure the value of  $\delta_{CP}$  is greatly enhanced by the knowledge of  
 544 the mass hierarchy we have also incorporated the expected data from the NO $\nu$ A experiment

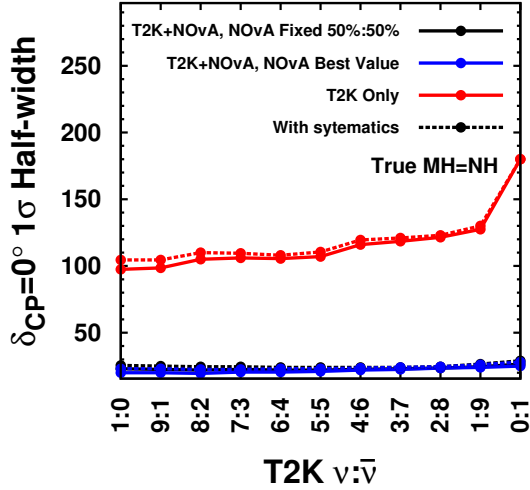
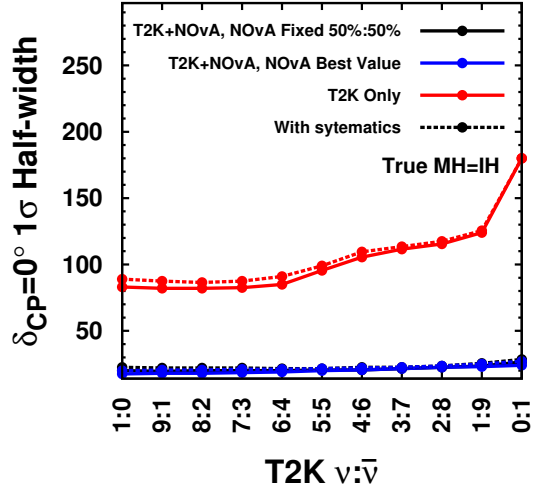
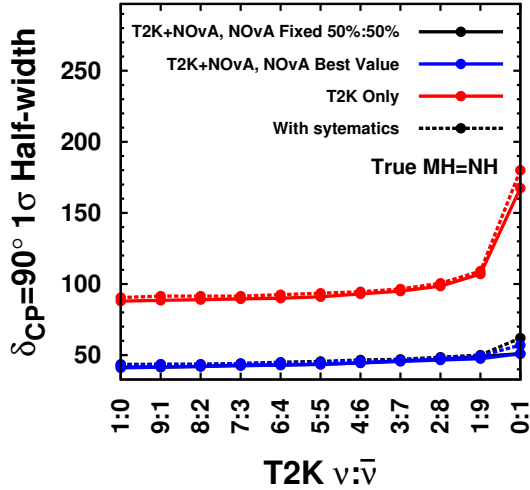
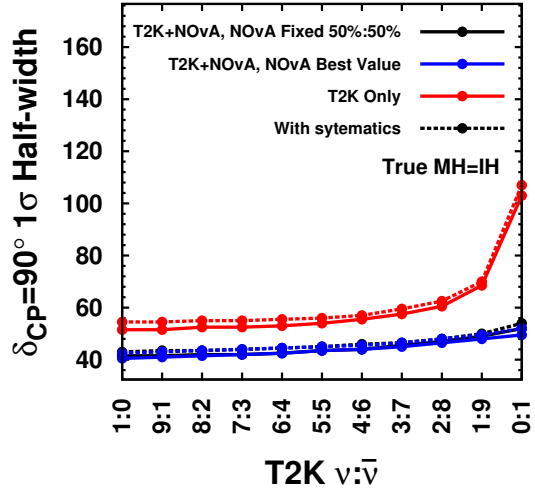
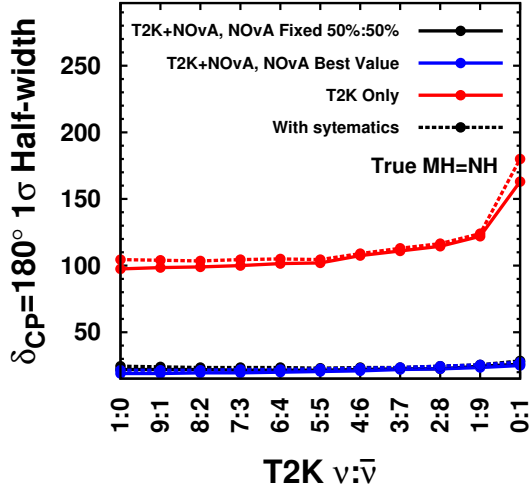
(a)  $\delta = 0^\circ$ , NH(b)  $\delta = 0^\circ$ , IH(c)  $\delta = 90^\circ$ , NH(d)  $\delta = 90^\circ$ , IH

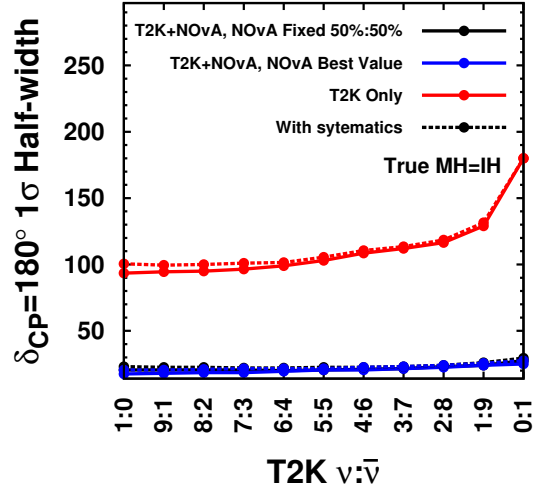
Fig. 26:  $\delta_{CP}$  resolution in a combined, T2K+NO $\nu$ A, fit as a function of T2K  $\nu:\bar{\nu}$  running ratio. Curves are given for the resolution value, in degrees, at nominal 5:5 NO $\nu$ A running (black), best case T2K+NO $\nu$ A running (blue), and T2K only running (red). Dashed (solid) curves indicate studies performed (without) assuming normalization systematics.

545 into our projections using the GLOBES tools. With the same normalization uncertainties of  
 546 5% on the signal and 10% on the background for both experiments we find, for example, that  
 547 the predicted  $\Delta\chi^2$  for rejecting the  $\delta_{CP} = 0$  hypothesis for  $\delta_{CP} = +90^\circ$ , IH and  $\sin^2 \theta_{23} = 0.5$   
 548 from the combined experiment fit is 8.2 compared to 4.3 and 3.2 for T2K and NO $\nu$ A alone,  
 549 respectively. The region of oscillation parameter space where there is sensitivity to observe  
 550 a non-zero  $\delta_{CP}$  is substantially increased compared to if each experiment is analyzed alone.

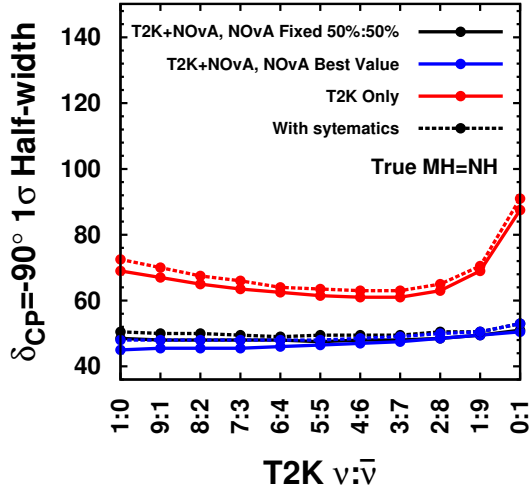
551 From the investigation of dividing the running time between  $\nu$ - and  $\bar{\nu}$ -modes we found  
 552 that an even split gives the best sensitivity for a wider region of the oscillation parameter



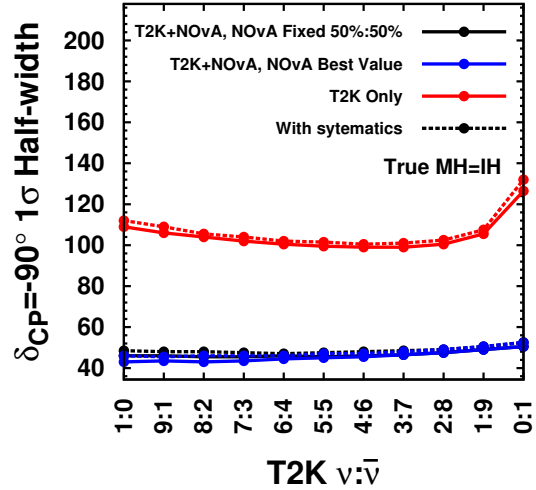
(a)  $\delta = 180^\circ$ , NH



(b)  $\delta = 180^\circ$ , IH



(c)  $\delta = -90^\circ$ , NH



(d)  $\delta = -90^\circ$ , IH

Fig. 27: Same as Fig. 26, but for different  $\delta_{CP}$  values.

553 space for both T2K data alone, and for T2K data in combination with  $\text{NO}\nu\text{A}$ , though the  
 554 dependence on the ratio is not strong.

555 It is anticipated that the results of these studies will help to guide the optimization of the  
 556 future run plan for T2K.

### Acknowledgment

557 We thank the J-PARC staff for superb accelerator performance and the CERN NA61  
 558 collaboration for providing valuable particle production data. We acknowledge the sup-  
 559 port of MEXT, Japan; NSERC, NRC and CFI, Canada; CEA and CNRS/IN2P3,  
 560 France; DFG, Germany; INFN, Italy; National Science Centre (NCN), Poland; RAS,  
 561 RFBR and MES, Russia; MICINN and CPAN, Spain; SNSF and SER, Switzerland;  
 562 STFC, UK; and DOE, USA. We also thank CERN for the UA1/NOMAD magnet,  
 563 DESY for the HERA-B magnet mover system, NII for SINET4, the WestGrid and



564 SciNet consortia in Compute Canada, GridPP, UK. In addition participation of indi-  
565 vidual researchers and institutions has been further supported by funds from: ERC  
566 (FP7), EU; JSPS, Japan; Royal Society, UK; DOE Early Career program, USA.

## 567 References

- 568 [1] Y. Fukuda et al., Phys. Rev. Lett., **81**, 1562–1567 (1998).  
569 [2] B.T. Cleveland, Timothy Daily, Jr. Davis, Raymond, James R. Distel, Kenneth Lande, et al.,  
570 Astrophys.J., **496**, 505–526 (1998).  
571 [3] K. Abe et al., Phys. Rev. D, **83**, 052010 (2011).  
572 [4] B. Aharmim et al., Phys. Rev. C, **88**, 025501 (2013).  
573 [5] G. Bellini et al., Phys. Rev. Lett., **108**, 051302 (2012).  
574 [6] K. Eguchi et al., Phys.Rev.Lett., **90**, 021802 (2003).  
575 [7] R. Wendell et al., Phys.Rev., **D81**, 092004 (2010).  
576 [8] P. Adamson et al., Phys. Rev. Lett., **110**, 251801 (2013).  
577 [9] K. Abe et al., Phys. Rev. Lett., **110**, 181802 (2013).  
578 [10] F. P. An et al., Phys. Rev. Lett., **108**, 171803 (2012).  
579 [11] Y. Abe et al., Phys. Rev. D, **86**, 052008 (2012).  
580 [12] J. K. Ahn and other, Phys. Rev. Lett., **108**, 191802 (2012).  
581 [13] M. H. Ahn et al., Phys. Rev. D, **74**, 072003 (2006).  
582 [14] K. Abe et al., Phys.Rev.Lett., **112**, 181801 (2014).  
583 [15] K. Abe et al., Phys. Rev. Lett., **107**, 041801 (2011).  
584 [16] K. Abe et al., Phys. Rev. D, **88**, 032002 (2013).  
585 [17] K. Abe et al., Phys.Rev.Lett., **112**, 061802 (2014).  
586 [18] P. Adamson et al., Phys. Rev. Lett., **110**, 171801 (2013).  
587 [19] N. Agafonova et al., Physics Letters B, **691**(3), 138 – 145 (2010).  
588 [20] Ziro Maki, Masami Nakagawa, and Shoichi Sakata, Prog.Theor.Phys., **28**, 870–880 (1962).  
589 [21] Letter of intent: Neutrino oscillation experiment at JHF (2003), [http://neutrino.kek.jp/jhfnu/loi/loi\\_JHFcor.pdf](http://neutrino.kek.jp/jhfnu/loi/loi_JHFcor.pdf).  
590 [22] K. Abe et al., Nucl. Instrum. Methods Phys. Res., Sect. A, **659**, 106–135, See Figure 16 for a schematic  
591 diagram of the ND280 detector. (2011).  
592 [23] Nova technical design report (), [http://www-nova.fnal.gov/nova\\_cd2\\_review/tdr\\_oct\\_23/tdr.htm](http://www-nova.fnal.gov/nova_cd2_review/tdr_oct_23/tdr.htm).  
593 [24] J. Arafune, M. Koike, and J Sato, Phys.Rev., **D56**, 3093–3099 (1997).  
594 [25] J. Beringer et al., Phys. Rev. D, **86**, 010001 (2012).  
595 [26] K. Abe et al., Phys. Rev. D, **87**, 012001 (2013).  
596 [27] K. Abe et al., Nucl. Instrum. Methods Phys. Res., Sect. A, **694**, 211–223 (2012).  
597 [28] S. Assylbekov et al., Nucl.Instrum.Meth., **A686**(0), 48 – 63 (2012).  
598 [29] N. Abgrall et al., Nucl. Instrum. Methods Phys. Res., Sect. A, **637**, 25–46 (2011).  
599 [30] P.A. Amaudruz et al., Nucl. Instrum. Methods Phys. Res., Sect. A, **696**, 1–31 (2012).  
600 [31] S. Aoki et al., Nucl.Instrum.Meth., **A698**, 135–146 (2013).  
601 [32] Y. Ashie et al., Phys. Rev. D, **71**, 112005 (2005).  
602 [33] N. Abgrall et al., Phys. Rev. C, **84**, 034604 (2011).  
603 [34] N. Abgrall et al., Phys. Rev. C, **85**, 035210 (2012).  
604 [35] K. Abe et al., Phys. Rev. D, **85**, 031103 (2012).  
605 [36] J. Beringer et al. (Particle Data Group), Phys. Rev., **D86**, 010001, 2013 partial update for the 2014  
606 edition (2012).  
607 [37] F. P. An et al., Chinese Physics C, **37**(1), 011001 (2013).  
608 [38] P. Huber, M. Lindner, and W. Winter, Computer Physics Communications, **167**(3), 195 – 202 (2005).  
609 [39] P. Huber, J. Kopp, M. Lindner, M. Rolinec, and W. Winter, Computer Physics Communications,  
610 **177**(5), 432 – 438 (2007).  
611 [40] [http://www-nova.fnal.gov/plots\\_and\\_figures/plot\\_and\\_figures.html](http://www-nova.fnal.gov/plots_and_figures/plot_and_figures.html) ().  
612 [41] <http://nova-docdb.fnal.gov/cgi-bin/ShowDocument?docid=7546> ().  
613 [42] <http://nova-docdb.fnal.gov/cgi-bin/ShowDocument?docid=7552> ().  
614 [43] X. Qian, A. Tan, W. Wang, J. J. Ling, R. D. McKeown, and C. Zhang, Phys. Rev. D, **86**, 113011 (Dec  
615 2012).  
616